

Antibacterial nucleoside-analog inhibitor of bacterial RNA polymerase: pseudouridimycin

Sonia I. Maffioli^{1,2,*}, Yu Zhang^{3,*}, David Degen^{3,*}, Thomas Carzaniga⁴, Giancarlo Del Gatto¹, Stefania Serina^{1,2}, Paolo Monciardini^{1,2}, Carlo Mazzetti¹, Paola Gugliera⁵, Gianpaolo Candiani², Alina Iulia Chiriac⁶, Giuseppe Facchetti², Petra Kaltofen², Hans-Georg Sahl⁶, Gianni Dehò⁴, Stefano Donadio^{1,2,**} and Richard H. Ebright^{3,**}

¹NAICONS Srl, 20139 Milan, Italy

²Vicuron Pharmaceuticals, 21040, Gerezano, Italy

³Waksman Institute and Department of Chemistry, Rutgers University, Piscataway NJ 08854, USA

⁴Department of Bioscience, University of Milan, 20122 Milan, Italy

⁵NeED Pharma Srl, 20139 Milan, Italy

⁶University of Bonn, D-53012 Bonn, Germany

*Contributed equally

**Corresponding authors: sdonadio@naicons.com; ebright@waksman.rutgers.edu

There is an urgent need for new antibacterial drugs effective against bacterial pathogens resistant to current drugs¹⁻². Nucleoside-analog inhibitors (NAIs) of viral nucleotide polymerases have had transformative impact in treatment of HIV³ and HCV⁴. NAIs of bacterial RNA polymerase (RNAP) potentially could have major impact on treatment of bacterial infection, particularly because functional constraints on substitution of RNAP nucleoside triphosphate (NTP) binding sites⁴⁻⁵ could limit resistance emergence⁴⁻⁵. Here we report the discovery, from microbial extract screening, of an NAI that inhibits bacterial RNAP and exhibits antibacterial activity against a broad spectrum of drug-sensitive and drug-resistant bacterial pathogens: pseudouridimycin (PUM). PUM is a novel microbial natural product consisting of a formamidinylated, N-hydroxylated Gly-Gln dipeptide conjugated to 6'-amino-pseudouridine. PUM potently and selectively inhibits bacterial RNAP in vitro, potently and selectively inhibits bacterial growth in culture, and potently clears infection in a mouse model of *Streptococcus pyogenes* peritonitis. PUM inhibits RNAP through a binding site on RNAP (the "i+1" NTP binding site) and mechanism (competition with UTP for occupancy of the "i+1" NTP binding site) that differ from those of the RNAP inhibitor and current antibacterial drug rifampin (Rif). PUM exhibits additive antibacterial activity when co-administered with Rif, exhibits no cross-resistance with Rif, and exhibits a spontaneous resistance rate an order-of-magnitude lower than that of Rif. The results provide the first example of a selective NAI of bacterial RNAP, provide an advanced lead compound for antibacterial drug development, and provide structural information and synthetic routes that enable lead optimization for antibacterial drug development.

We screened a library of 3000 Actinobacterial⁶ and fungal culture extracts for inhibition of RNAP, and we identified two extracts that inhibited bacterial RNAP (*E. coli* RNAP) but did not inhibit a structurally unrelated bacteriophage RNAP (SP6 RNAP) and did not contain a previously characterized inhibitor of bacterial RNAP (see Methods). Fractionation of the two extracts by reversed-phase chromatography and structure elucidation of active components by mass spectrometry and

multidimensional NMR spectrometry revealed that the extracts contained the same novel active component: pseudouridimycin (PUM; Fig. 1a; Extended Data Figs. 1-2).

PUM selectively inhibits bacterial RNAP ($IC_{50} = 0.1 \mu M$; selectivity >4- to >500-fold; Fig. 1b; Extended Data Table 1; Extended Data Fig. 3), selectively inhibits bacterial growth ($IC_{50} = 2$ to $16 \mu M$; selectivity >6- to >60-fold; Fig. 1c), and clears infection *in vivo* in a mouse *Streptococcus pyogenes* peritonitis model ($ED_{50} = 9$ mg/kg; Fig. 1c; Extended Data Table 2). PUM exhibits antibacterial activity against both Gram-positive and Gram-negative bacteria and against both drug-sensitive and drug-resistant bacterial strains, including rifamycin-, β -lactam-, fluoroquinolone- macrolide-, tetracycline-, aminoglycoside-, lincosamide-, chloramphenicol-, oxazolidinone-, trimethoprim-, glycopeptide-, lipopeptide-, mupirocin-, and multi-drug-resistant strains (Fig. 1c).

PUM exhibits no cross-resistance with the classic RNAP inhibitor Rif (Figs. 1b-c,e), exhibits additive antibacterial activity when co-administered with Rif (Fig. 1f), and exhibits spontaneous resistance rates an order-of-magnitude lower than those of Rif (Fig. 2a), suggesting that PUM inhibits RNAP through a binding site and mechanism different from those of Rif.

Gene sequencing indicates that PUM-resistant mutants contain mutations in the *rpoB* gene (encodes RNAP β subunit) or the *rpoC* gene (encodes RNAP β' subunit), confirming that RNAP is the functional cellular target of PUM (Fig. 2b; Extended Data Fig. 4a-b). In the Gram-positive bacterium *S. pyogenes*, substitutions conferring ≥ 4 x PUM-resistance are obtained at four sites: β residues 565, 681, and 684, and β' residue 786 (numbered as in *E. coli* RNAP; Fig. 2b). In the Gram-negative bacterium *E. coli*, substitutions conferring PUM-resistance are obtained at two sites: β residues 565 and 681 (Extended Data Fig. 4a-b). The number of sites of substitutions conferring PUM-resistance is an order-of-magnitude lower than the number of sites of substitutions conferring Rif-resistance (2 to 4 vs. 25^{7-8}), consistent with, and accounting for, the observation that spontaneous resistance rates for PUM are an order-of-magnitude lower than those for Rif (Fig. 2a).

Mapping the sites of substitutions conferring PUM resistance onto the three-dimensional structure of bacterial RNAP shows that the sites form a single discrete cluster ("PUM target"; Fig. 2c; Extended Data Fig. 4d). The PUM target is located within the RNAP active-center region and overlaps the RNAP active-center i+1 NTP binding site (Fig. 2c; Extended Data Fig. 4d), suggesting that PUM inhibits RNAP by interfering with function of the i+1 site. The PUM target is different from, and does not overlap, the Rif target (Fig. 2d; Extended Data Fig. 4e)⁷⁻⁹, consistent with, and accounting for, the observation that PUM does not share cross-resistance with Rif (Figs. 1b-c,e, 2e; Extended Data Fig. 4f-g) and the observation that PUM and Rif exhibit additive antibacterial activity (Fig. 1f). The PUM target also is different from, and does not overlap, the targets of the RNAP inhibitors lipiarmycin (Lpm)¹⁰⁻¹¹, myxopyronin (Myx)¹¹⁻¹³, streptolydigin (Stl)¹⁴⁻¹⁵, CBR703 (CBR)¹⁶⁻¹⁷, and salinamide (Sal)¹⁸ (Fig. 2d; Extended Data Fig. 4e), and, correspondingly, PUM does not exhibit cross-resistance with Lpm, Myx, Stl, CBR703, and Sal (Fig. 2e; Extended Data Fig. 4f,h-l). The PUM target partly overlaps the target for the RNAP inhibitor GE23077 (GE; Extended Data Fig. 4m)⁵, and, correspondingly, PUM exhibits partial cross-resistance with GE (Extended Data Fig. 4n).

The observation that PUM is an NAI that has the same Watson-Crick base-pairing specificity as UTP (Fig. 1a) and the observation that the PUM target overlaps the RNAP i+1 NTP binding site (Fig. 2b; Extended Data Fig. 4a) suggest the hypothesis that PUM functions as an NAI that competes with UTP for occupancy of the RNAP i+1 NTP binding site. Five biochemical results support this hypothesis. First, PUM inhibits transcription by inhibiting nucleotide addition (Extended Data Fig. 5). Second, high concentrations of UTP--but not high concentrations of GTP, ATP, or CTP--overcome transcription inhibition by PUM (Fig. 3a). Third, PUM inhibits transcription only on templates that direct incorporation of U (Fig. 3b). Fourth, in single-nucleotide-addition transcription reactions, PUM inhibits incorporation of U, but not G, A, or C (Fig. 3c). Fifth, in multiple-nucleotide-addition transcription reactions, PUM inhibits incorporation of U, but not G, A, or C (Fig. 3d). The results in Fig. 3c-d further establish that transcription inhibition by PUM not only requires a template position that directs incorporation of U, but also strongly prefers a preceding template position that directs incorporation of G, A, or U. We conclude

that PUM functions as an NAI that competes with UTP at positions that direct incorporation of U preceded by positions that direct incorporation of G, A, or U.

To define the structural basis of transcription inhibition by PUM, we determined a crystal structure of a transcription initiation complex containing PUM (R_{Po}-GpA-PUM; Fig. 4a) and, for comparison, a crystal structure of a corresponding transcription initiation complex containing CMPcPP (R_{Po}-GpA-CMPcPP; Fig. 4b). The results establish that PUM is an NAI that competes for occupancy of the *i*+1 site (Fig. 4). PUM binds to the *i*+1 site (Fig. 4a). The PUM base makes Watson-Crick H-bonds with a DNA template-strand A in a manner equivalent to an NTP base; the PUM sugar moiety makes interactions with the *i*+1 site in a manner nearly equivalent to an NTP sugar; the PUM glutamine moiety makes interactions that mimic interactions made by an NTP triphosphate; and the PUM N-hydroxy and guanidinyI moieties interact with the RNA nucleotide base-paired to the preceding template position (RNA 3'-nucleotide), with the N-hydroxy donating an H-bond to the 3'-OH of the RNA 3'-nucleotide, and the guanidinyI moiety donating one H-bond to the 5'-phosphate of the RNA 3'-nucleotide and another to the base of the RNA 3'-nucleotide (Fig. 4a).

The structure of the PUM-inhibited complex accounts for the observed specificity of inhibition for template positions that direct incorporation of U preceded by template positions that direct incorporation of G, A, or U. The Watson-Crick base pair by the PUM base moiety provides absolute specificity for a position directing incorporation of U (Fig. 4a). The H-bond donated by the PUM guanidinyI moiety with the base of the RNA 3'-nucleotide confers specificity for a preceding position directing incorporation of G, A, or U (each of which contains an H-bond acceptor at the appropriate position; Fig. 4a).

The structure also explains the selectivity of transcription inhibition by PUM. All RNAP residues contacted by PUM are highly conserved across Gram-positive and Gram-negative bacterial RNAP (Extended Data Fig. 6), accounting for the inhibition of both Gram-positive and Gram-negative bacterial RNAP. In contrast, four RNAP residues important for PUM are not conserved in human RNAP I, II, and

III (β residues 677, 681, and 684, and β' residue 932; Extended Data Fig. 6), accounting for selectivity for bacterial RNAP over human RNAP I, II, and III.

The structure also explains the small size of the PUM resistance spectrum (four residues in *S. pyogenes* RNAP; two residues in *E. coli* RNAP; Fig. 2b; Extended Data Fig. 4a-b). PUM makes direct contacts with RNAP residues at which PUM-resistant substitutions are obtained (Extended Data Fig. 6). However, PUM also makes direct contacts with ten other RNAP residues that comprise functionally critical residues of the RNAP active center that cannot be substituted without compromising RNAP activity^{5;19-23}, and thus which cannot be substituted to yield viable resistant mutants⁵ (Fig. 4a). We infer that PUM interacts with a "*privileged target*" for which most residues (10-12 of 14 residues) have functional constraints that limit substitution to yield viable resistant mutants. Similar results have been reported for the RNAP inhibitor GE, a non-nucleoside-analog inhibitor that binds to the RNAP i and i+1 sites⁵ and that exhibits a small target-based resistance spectrum⁵ (but that, unlike PUM, exhibits high non-target-based resistance, presumably at the level of uptake or efflux, precluding development as an antibacterial drug).

The structure enables structure-based design of novel PUM analogs with increased potency and increased selectivity. Initial lead-optimization efforts corroborate the importance of the PUM N-hydroxy, glutamine, and guanidinyll moieties and demonstrate that the PUM glutamine C(O)NH₂ can be replaced by C(O)NHR while retaining RNAP inhibitory and antibacterial activity (Extended Data Fig. 7).

Our results provide a new class of antibiotic with activity against Gram-positive and Gram-negative bacteria *in vitro* and *in vivo*, no cross-resistance with current antibacterial drugs, and low rates of resistance emergence. Our discovery of a new class of antibiotic from conventional microbial extract screening indicates that, contrary to widespread belief⁴, conventional microbial extract screening has not been exhausted as a source of new antibacterial lead compounds.

Our results provide the first example of a selective NAI of bacterial RNAP. NAIs of viral nucleotide polymerases have been of immense importance for development of anti-HIV³ and anti-HCV⁴ drugs. NAIs of bacterial RNAP may show comparable promise for development of antibacterial drugs.

References

1. Marston, H., Dixon, D., Knisely, J., Palmore, T. & Fauci, A. Antimicrobial resistance. *JAMA* **316**, 1193-1204 (2016).
2. Brown, E. & Wright, G. Antibacterial drug discovery in the resistance era. *Nature* **529**, 336-343 (2016).
3. Cihlar, T. & Ray, A. Nucleoside and nucleotide HIV reverse transcriptase inhibitors: 25 years after zidovudine. *Antiviral Res.* **85**, 39-58 (2010).
4. Summers, B., Beavers, J. & Klibanov, O. Sofosbuvir [Solvadi], a novel nucleotide analogue inhibitor used for the treatment of hepatitis C virus. *J. Pharm. Pharmacol.* **66**, 1653-1666 (2014).
5. Zhang, Y., Degen, D., Ho, M., Sineva, E., Ebright, K., Ebright, Y., Mekler, V., Vahedian-Movahed, H., Feng, Y., Yin, R., Tuske, S., Irschik, H., Jansen, R., Maffioli, S., Donadio, S., Arnold, E. & Ebright, R.H. GE23077 binds to the RNA polymerase 'i' and 'i+1' sites and prevents the binding of initiating nucleotides. *eLife* **3**, e02450 (2014).
6. Landwehr, W., Wolf, C. & Wink, J. Actinobacteria and Myxobacteria: two of the most important bacterial resources for novel antibiotics. *Curr. Top. Microbiol. Immunol.* **398**, 273-302 (2016).
7. Jin, D. J. & Gross, C. Mapping and sequencing of mutations in the *Escherichia coli* *rpoB* gene that lead to rifampicin resistance. *J. Mol. Biol.* **202**, 45-58 (1988).
8. Garibyan, L., Huang, T., Kim, M., Wolff, E., Nguyen, A., Nguyen, T., Diep, A., Hu, K., Iverson, A., Yang, H. & Miller, J. Use of the *rpoB* gene to determine the specificity of base substitution mutations on the *Escherichia coli* chromosome, *DNA Repair* **2**, 593-608 (2003).
9. Campbell, E., Korzheva, N., Mustaev, A., Murakami, K., Nair, S., Goldfarb, A. & Darst, S. Structural mechanism for rifampicin inhibition of bacterial RNA polymerase. *Cell* **104**, 901-912 (2001).
10. Ebright, R. RNA exit channel--target and method for inhibition of bacterial RNA polymerase. *WO/2005/001034* (2005).

11. Srivastava, A., Talaue, M., Liu, S., Degen, D., Ebright, R.Y., Sineva, E., Chakraborty, A., Druzhinin, S., Chatterjee, S., Mukhopadhyay, J., Ebright, Y., Zozula, A., Shen, J., Sengupta, S., Niedfeldt, R., Xin, C., Kaneko, T., Irschik, H., Jansen, R., Donadio, S., Connell, N. & Ebright, R.H. New target for inhibition of bacterial RNA polymerase: "switch region". *Curr. Opin. Microbiol.* **14**, 532-543 (2011).
12. Mukhopadhyay, J., Das, K., Ismail, S., Koppstein, D., Jang, M., Hudson, B., Sarafianos, S., Tuske, S., Patel, J., Jansen, R., Irschik, H., Arnold, E. & Ebright, R.H. The RNA polymerase "switch region" is a target for inhibitors. *Cell* **135**, 295-307 (2008).
13. Belogurov, G., Vassilyeva, M., Sevostyanova, A., Appleman, J., Xiang, A., Lira, R., Webber, S., Klyuyev, S., Nudler, E., Artsimovitch, I. & Vassilyev, D. Transcription inactivation through local refolding of the RNA polymerase structure. *Nature* **45**, 332-335. (2009).
14. Tuske, S., Sarafianos, S., Wang, X., Hudson, B., Sineva, E., Mukhopadhyay, J., Birktoft, J., Leroy, O., Ismail, S., Clark, A., Dharia, C., Napoli, A., Liptenko, O., Lee, J., Borukhov, S., Ebright, R.H. & Arnold, E. Inhibition of bacterial RNA polymerase by streptolydigin: stabilization of a straight-bridge-helix active-center conformation. *Cell* **122**, 541-552 (2005).
15. Temiakov, D., Zenkin, N., Vassilyeva, M., Perederina, A., Tahirov, T., Kaihatsu, K., Savkina, M., Zorov, S., Nikiforov, V., Igarashi, N., Matsugaki, N., Wakatsuki, S., Severinov, K. & Vassilyev, D. Structural basis of transcription inhibition by antibiotic streptolydigin. *Mol. Cell* **19**, 655-666 (2005).
16. Feng, Y., Degen, D., Wang, X., Gigliotti, M., Liu, S., Zhang, Y., Das, D., Michalchuk, T., Ebright, Y., Talaue, M., Connell, N. & Ebright, R.H. Structural basis of transcription inhibition by CBR hydroxamides and CBR pyrazoles. *Structure* **23**, 1470-1481 (2015).
17. Bae, B., Nayak, D., Ray, A., Mustaev, A., Landick, R. & Darst, S. CBR antimicrobials inhibit RNA polymerase via at least two bridge-helix cap-mediated effects on nucleotide addition. *Proc. Natl. Acad. Sci. USA* **112**, E4178-E4187 (2015).

18. Degen, D., Feng, Y., Zhang, Y., Ebright, K., Ebright, Y., Gigliotti, M., Vahedian-Movahed, H., Mandal, S., Talaue, M., Connell, N., Arnold, E., Fenical, W. & Ebright, R.H. Transcription inhibition by the depsipeptide antibiotic salinamide A. *eLife* **3**, e02451 (2014).
21. Sagitov, V., Nikiforov, V. & Goldfarb, A. Dominant lethal mutations near the 5' substrate binding site affect RNA polymerase propagation. *J. Biol. Chem.* **268**, 2195-2202. (1993).
22. Svetlov, V., Vassilyev, D. & Artsimovitch, I. Discrimination against deoxyribonucleotide substrates by bacterial RNA polymerase. *J. Biol. Chem.* **279**, 38087-38090 (2004).
21. Sosunov, V., Zorov, S., Sosunova, E., Nikolaev, A., Zakeyeva, I., Bass, I., Goldfarb, A., Nikiforov, V., Severinov, K. & Mustaev, A. The involvement of the aspartate triad of the active center in all catalytic activities of multisubunit RNA polymerase. *Nucl. Acids Res.* **33**, 4202-4211 (2005).
22. Jovanovic, M., Burrows, P., Bose, D., Cámara, B., Wiesler, S., Weinzierl, R., Zhang, X., Wigneshweraraj, S. & Buck, M. An activity map of the *Escherichia coli* RNA polymerase bridge helix. *J. Biol. Chem.* **286**, 14469-14479 (2011).
23. Yuzenkova, Y., Roghanian, M. & Zenkin, N. Multiple active centers of multi-subunit RNA polymerases. *Transcription* **3**, 115-118 (2012).

Acknowledgements

Work was supported by NIH grants GM041376 and AI104660 to RHE and Italian Ministry of Research and Regione Lombardia grants to NAICONs. We thank former colleagues at Vicuron Pharmaceuticals for early characterization of PUM, S. Parapini for cytotoxicity assays, W. Fenical for Sal, A. Berk and I. Grummt for plasmids, NARSA and BEI Resources for strains, and the Cornell High Energy Synchrotron Source for beamline access.

Data Availability

Atomic coordinates and structure factors for reported crystal structures have been deposited with the Protein Data Bank under accession codes 5X21 (RPO-GpA-PUM) and 5X22 (RPO-GpA-CMPcPP).

Author Contributions

S.M. performed structure elucidation of PUM and semi-syntheses and syntheses of PUM derivatives. Y.Z. purified RNAP, assessed template-specificity of inhibition and determined crystal structures. D.D. purified RNAP, and assessed RNAP-inhibitory activities, antibacterial activities, resistance, and cross-resistance. T.C., S.S., and G.D. assessed RNAP-inhibitory activities. G.D.G. and C.M. purified PUM and participated in semi-syntheses and syntheses of PUM derivatives. P.M. performed characterization and fermentation of the PUM producer strain. P.G. and G.C. performed mouse infection studies. A.I.C. and H.-G.S. performed macromolecular synthesis assays. G.F. and P.K. performed microbial extract screening and dereplication. S.D. and R.H.E. designed the study, analyzed data, and wrote the paper.

Author Information

S.M., S.S., P.M., and S.D. are employees and/or shareholders of NAICONs. Y.Z., S.M., S.S., P.M., P.G., G.C., S.D., and R.H.E. have patent filings. The other authors declare that no competing interests exist. (Vicuron Pharmaceuticals no longer is operational.) Correspondence and requests for materials should be addressed to S.D. (sdonadio@naicons.com) or R.H.E. (ebright@waksman.rutgers.edu).

Figure Legends

Figure 1. Structure, RNAP-inhibitory activity, and antibacterial activity of PUM.

a, Structure of PUM. **b**, RNAP-inhibitory activity of PUM. **c**, Antibacterial activity of PUM *in vitro*. **d**, Antibacterial activity of PUM *in vivo*. Drug resistances are as follows: Ami, amikacin; Azi, azithromycin; Cip, ciprofloxacin; Ctr, ceftriaxone; Dap, daptomycin; Ery, erythromycin; Chl, chloramphenicol; Cli, clindamycin; Gen, gentamycin; Lin, linezolid; Met, methicillin; Mup, mupirocin; Pen, penicillin; Ox, oxacillin; Rif, rifampin; Tec, teicoplanin; Tet, tetracycline; Tri, trimethoprim; Van, vancomycin. **e**, Absence of cross-resistance between PUM and Rif (data for *S. pyogenes* Rif-resistant mutants; residues numbered as in *S. pyogenes* and, in parentheses, *E. coli*). **f**, Additive antibacterial activity of PUM and Rif.

Figure 2. Target of PUM: RNAP i+1 NTP binding site.

a, Spontaneous resistance rates for PUM and Rif. **b**, *S. pyogenes* spontaneous PUM-resistant mutants. **c**, Location of PUM target (blue) in three-dimensional structure of bacterial RNAP¹² (gray; black circle for active-center region; violet sphere for active-center Mg²⁺(I); β' non-conserved region and σ omitted for clarity). **d**, Absence of overlap between PUM target (blue) and Rif (red), Lpm (cyan), Myx (pink), and Stl (yellow) targets. **e**, Absence of high-level cross-resistance for *S. pyogenes* PUM-resistant mutants to Rif, Lpm, Myx, and Stl.

Figure 3. Mechanism of PUM: competition with UTP for occupancy of RNAP i+1 NTP binding site.

a, Suppression of inhibition by PUM by high [UTP], but not high [GTP], [ATP], or [CTP]. **b**, Inhibition by PUM of transcription directing incorporation of U+G+A+C, but not "U-less" transcription specifying incorporation of G+A+C. **c**, Single-nucleotide-addition reactions showing that inhibition by PUM requires template positions directing incorporation of U (row 1) and prefers preceding template positions directing incorporation of G, A, or U (columns 1-3). **d**, Multiple-nucleotide-addition reactions showing

that inhibition by PUM requires template positions directing incorporation of U (red GU, AU, or UU, and pink CU) and prefers preceding template positions directing incorporation of G, A, or U (red GU, AU, or UU).

Figure 4. Structural basis of transcription inhibition by PUM

Structures of transcription initiation complexes containing PUM (**a**) and CMPcPP (**b**). Top, crystallization and refinement statistics (left) and experimental electron density and fit (right). Green, PUM; pink, RNA and CMPcPP; red, DNA template strand; violet sphere between *i* and *i*+1 sites, Mg²⁺(I); violet sphere in *i*+1 site, Mg²⁺(II); gray, RNAP bridge helix; green mesh, mF_o-DF_c omit map (contoured at 2.5σ). Middle, stereodiagram of interactions. Green, PUM carbon atoms; pink, RNA and CMPcPP carbon atoms; gray, RNAP carbon atoms; red, blue, yellow, and orange, oxygen, nitrogen, sulfur, and phosphorous atoms; dashed lines, H-bonds; other colors, as above. Bottom, summary of interactions. Red dashed lines, H-bonds; blue arcs, van der Waals interactions. Residues numbered as in *T. thermophilus* RNAP and, in parentheses, *E. coli* RNAP.



Figure 1

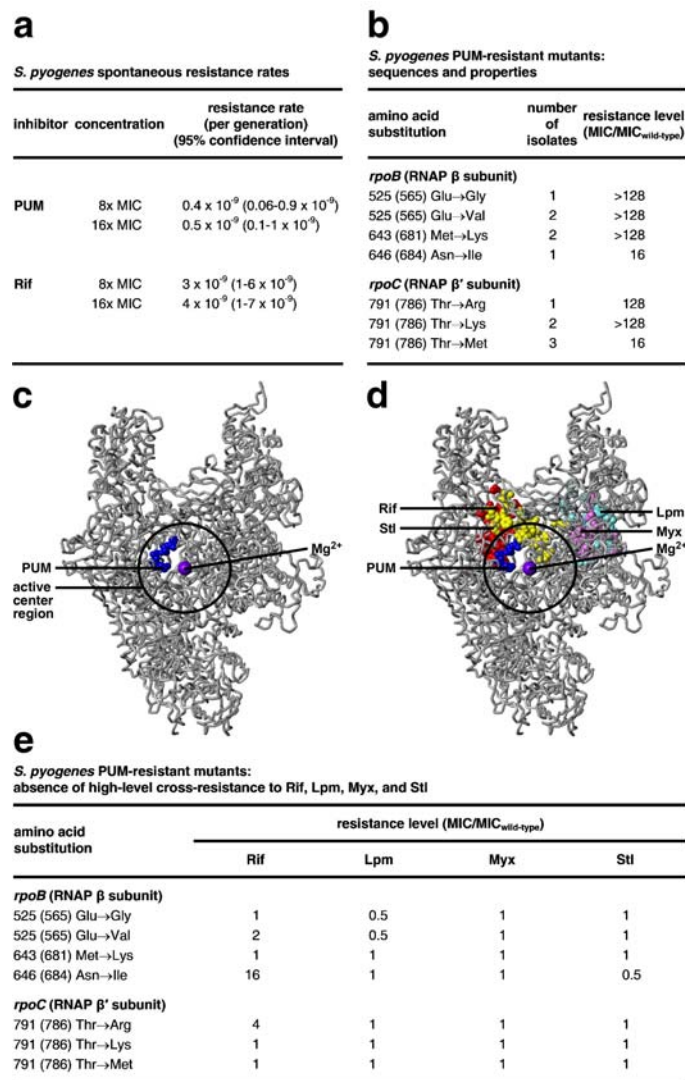


Figure 2

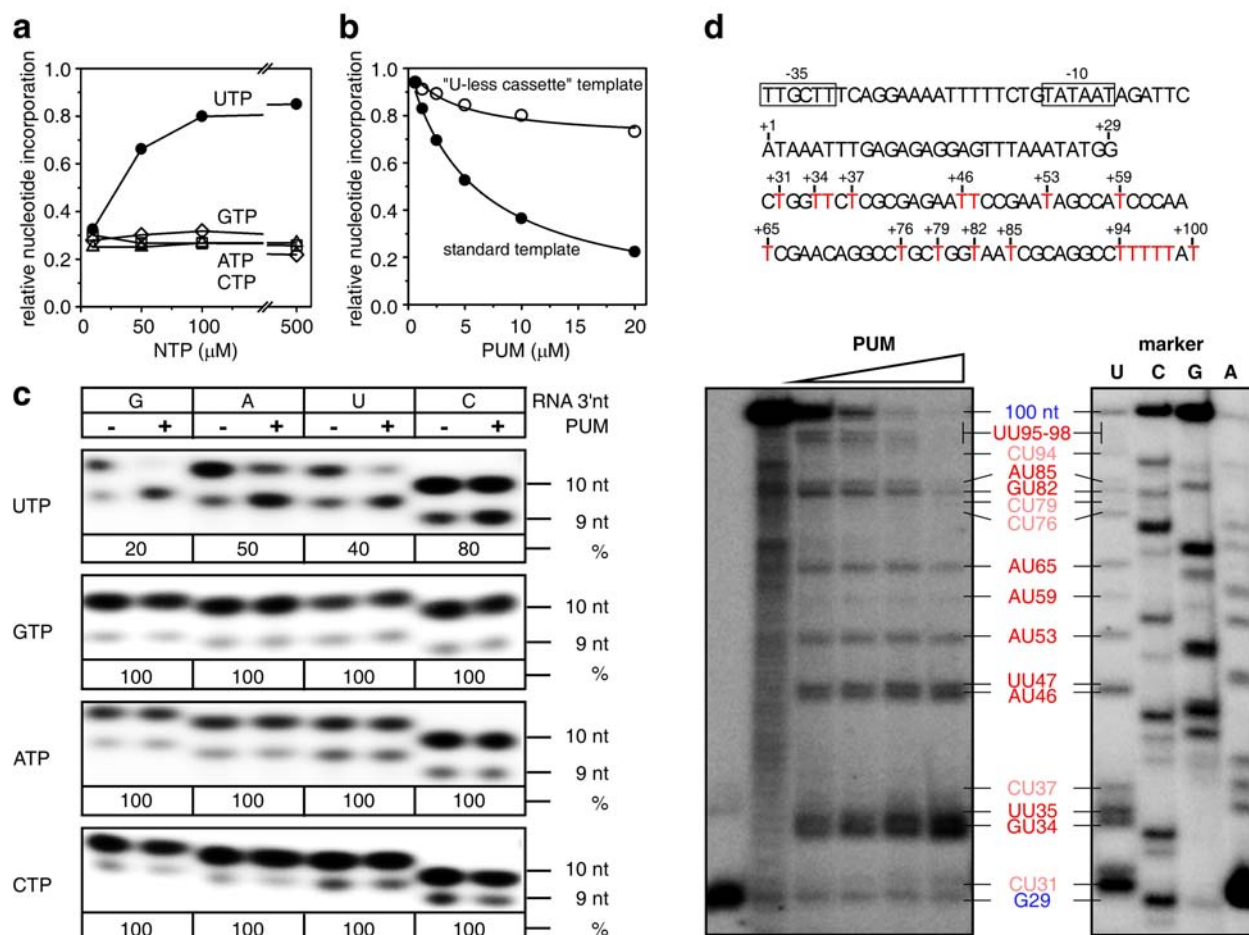


Figure 3

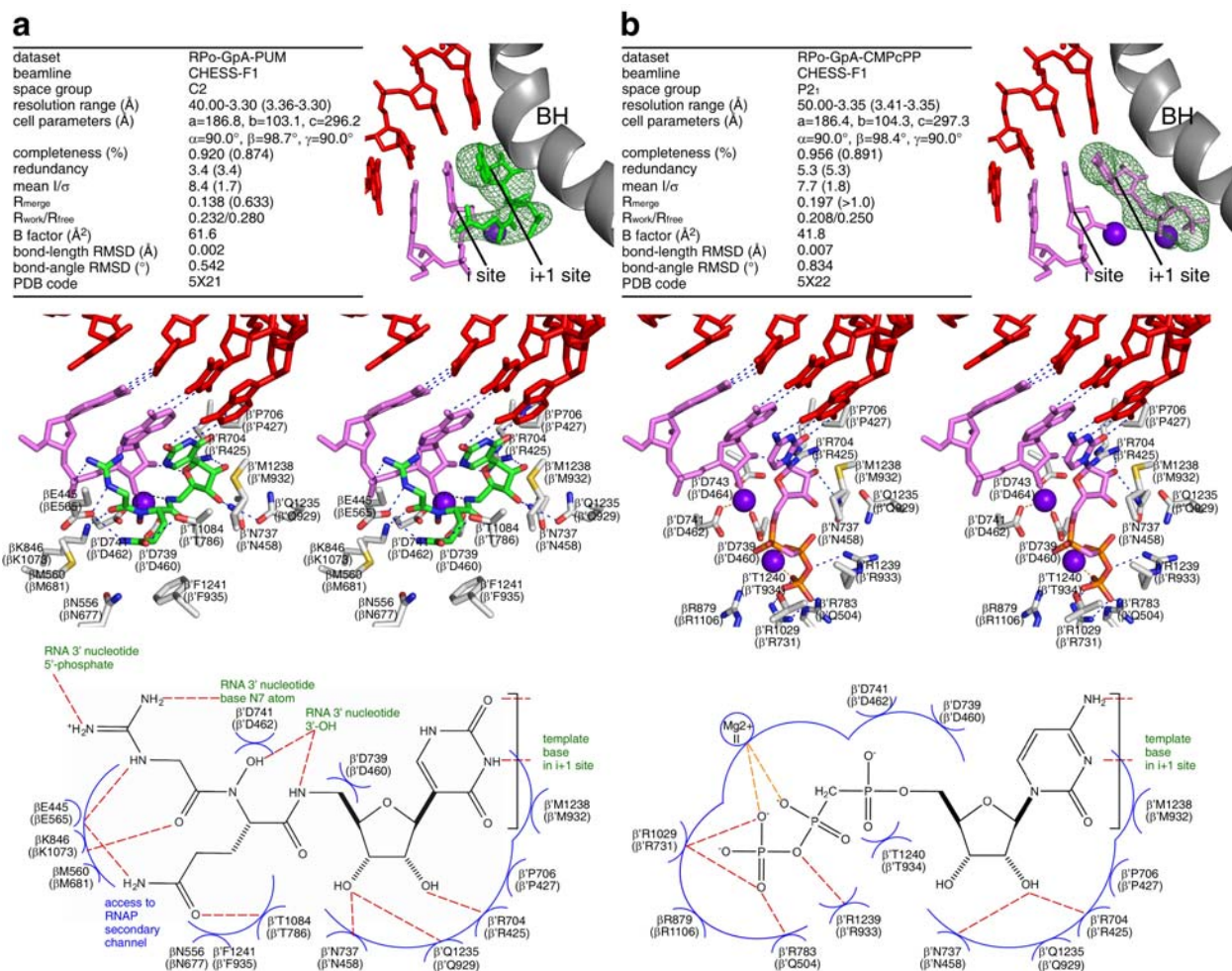


Figure 4

METHODS

E. coli RNAP core enzyme

For experiments in Fig. 3c, *E. coli* RNAP core enzyme was prepared from *E. coli* strain BL21(DE3) (Invitrogen) transformed with plasmids pEcABC-H6²⁴ and pCDFω²⁵, using procedures as described²⁶.

For experiments assessing promoter-independent transcription in Extended Data Table 1, *E. coli* RNAP core enzyme was prepared from *E. coli* strain XE54²⁷ transformed with plasmid pRL706²⁸, using procedures as described²⁹.

E. coli RNAP σ⁷⁰ holoenzyme

For experiments in Fig. 3d, *E. coli* RNAP σ⁷⁰ holoenzyme was prepared from *E. coli* strain XE54²⁶ transformed with plasmid pREII-NHα²⁹, using procedures as described¹⁸.

For experiments in Extended Data Fig. 4c, *E. coli* RNAP σ⁷⁰ holoenzyme and [565Glu→Asp]β-RNAP σ⁷⁰ holoenzyme were prepared from *E. coli* strain XE54²⁶ transformed with plasmid pRL706²⁸ or pRL706-565D⁵, using procedures as described²⁹.

B. subtilis RNAP σ^A holoenzyme

Rif-resistant *B. subtilis* [469 (513) Gln→Arg]β-RNAP σ^A holoenzyme was prepared from *B. subtilis* strain MH5636-Q469R (spontaneous Rif-resistant mutant of *B. subtilis* strain MH5636³⁰; selected on LB agar containing 2 μg/ml Rif; confirmed by PCR amplification and sequencing of *rpoB*) using procedures essentially as described³⁰.

T. thermophilus RNAP σ^A holoenzyme

T. thermophilus RNAP σ^A holoenzyme was prepared as described⁵.

Microbial extract screening

A sub-library of ~3,000 microbial extracts (prepared as described³¹) with growth-inhibitory activity against *Staphylococcus aureus* ATCC 6538 was screened for the ability to inhibit *E. coli* RNAP and bacteriophage SP6 RNAP (Promega). Screening was performed using 96-well microplates. Reactions contained (50 μl): 5 μl extract (dissolved in 10% DMSO), 0.2 U *E. coli* RNAP σ⁷⁰ holoenzyme (Sigma-Aldrich) or 0.2 U SP6 RNAP (Promega), 0.2 nM plasmid pUC18 (Clontech; for assays with *E. coli* RNAP) or 0.2 nM plasmid pGEM-3Z (Promega; for assays with SP6 RNAP), 500 μM ATP, 500 μM GTP, 500 μM CTP, and 2 μM [α³²P]UTP (0.2 Bq/fmol; PerkinElmer), in 20 mM Tris-acetate (pH 7.9), 50 mM KCl, 4 mM magnesium acetate, 0.1 mM EDTA, 5 mM dithiothreitol, and 100 μg/ml bovine serum albumin. Reaction components except DNA were pre-equilibrated 10 min at 22°C. Reactions were initiated by addition of DNA, were allowed to proceed 1 h at 22°C, and were terminated by addition of 150 μl ice-cold 10% (w/v) trichloroacetic acid (TCA). After 1 h at 4°C, resulting TCA precipitates were collected on glass-fiber filters (UniFilter GF/B; PerkinElmer) using a 96-well harvester (Packard) and were washed once with water. Radioactivity was quantified using a TopCount scintillation counter (Packard), and % inhibition was calculated as:

$$\% \text{ inhibition} = 100 - [100(R_{\text{sample}} - R_{\text{neg}})/(R_{\text{pos}} - R_{\text{neg}})]$$

where R_{sample} , R_{pos} and R_{neg} are observed radioactivity levels in a reaction, in a control reaction without extract, and in a control reaction without plasmid, respectively.

Two extracts that inhibited the reaction with *E. coli* RNAP by ≥80%, that did not inhibit the reaction with SP6 RNAP, and that did not contain mass-spectrometry signals indicative of a previously characterized RNAP inhibitor, were designated as "hit extracts."

Characterization of producer strains

The producer strains of the hit extracts were strains IDI38640 and IDI38673. ID38640 and ID38673 are Actinobacterial isolates from soil samples collected in Italy and France, respectively. ID38640 and ID38673 exhibit cell morphologies consistent with the genus *Streptomyces* and exhibit 16S rRNA gene sequences (determined as described³²; GenBank accession numbers JQ929050 and JQ929051) that were 99.9% identical over 1.4 kB to each other and were highly similar to those of a cluster of closely-related *Streptomyces* species (*S. nigrescens*, *S. tubercidicus*, *S. rimosus* subsp. *rimosus*, *S. hygroscopicus* subsp. *angustmyceticus*, and *S. libani* subsp. *libani*).

Isolation and purification of PUM

For each producer strain of a hit extract, the strain was cultured on a 55 mm BTT agar plate³¹ 4-7 days at 30°C, the mycelium was scraped from the plate and used to inoculate a 50 ml Erlenmeyer flask containing 15 ml of seed medium (20 g/L dextrose monohydrate, 2 g/L yeast extract, 8 g/L soybean meal, 1 g/L NaCl, and 4 g/L CaCO₃, pH 7.3), and the resulting culture was incubated 48 h at 30°C on a rotary shaker (200 rpm agitation) for 48 h. Following initial incubation, 5 ml of the culture was used to inoculate 100 ml of fresh seed medium in a 500-ml flask, and the resulting culture was incubated 72 h under the same conditions. A 5% (v/v) inoculum was transferred into 2 L of production medium (10 g/L dextrose monohydrate, 24 g/L maize dextrin, 8 g/L soy peptone, 5 g/L yeast extract, and 1 g/L NaCl, pH 7.2) in a 3-L vessel, and the resulting culture was grown in a BioFlo 115 Fermentor (Eppendorf) 96 h at 30°C, with aeration at 0.5 volume air per volume medium per min stirring at 600 rpm. The culture was filtered through 10.25 in disc filter paper (Scienceware), and the resulting cleared broth was concentrated to ~1 L *in vacuo* and loaded onto a column of 500 mg of Dowex 50W x 400 mesh (previously activated with two bed volumes of 5% HCl and washed with H₂O until neutralization). After washing with 5 bed volumes each of 20 mM sodium acetate at pH 6 and sodium acetate at pH 7, PUM was eluted using six bed volumes of 100 mM NH₄OAc at pH 9. PUM-containing fractions were desalted by reversed-phase medium-pressure liquid chromatography on Combiflash Rf (Teledyne Isco) using a 30 g C18 RediSep Rf column (Teledyne Isco) with linear gradient from 0 to 20% phase B in 20 min (phase A, 0.02% trifluoroacetic acid in H₂O; phase B, acetonitrile) and flow rate of 35 ml/min. PUM-containing fractions were pooled, concentrated, and lyophilized twice to yield 196 mg of a white solid highly soluble in water, DMSO, and methanol.

Structure elucidation of PUM

Ion-trap ESI-MS (Bruker Esquire 3000 Plus) showed a protonated molecular ion at m/z 487 [M+H]⁺ and a bimolecular ion at 973 [2M+H]⁺ (Extended Data Fig. 1). Ion-trap ESI-MS/MS (Bruker Esquire 3000 Plus) showed major peaks at m/z 334, 353, 371, 389, 452, and 479 [M+H]⁺. HR-MS (Thermo Fisher Exactive) showed an exact mass of 487.18865, consistent with the molecular formula C₁₇H₂₆N₈O₉.

Reversed-phase HPLC (Shimadzu Series 10 with SPD-M10A VP diode array detector; Waters Symmetry Shield RP8 5μm, 250 x 4.6 mm, column; phase A = 2 mM heptafluorobutyric acid in water; phase B = 2 mM heptafluorobutyric acid in acetonitrile; gradient = 0% B at 0 min, 10% B at 20 min, 95% B at 30 min; flow rate = 1 ml/min) showed a single peak with a retention time of 12 minutes. The UV-absorbance spectrum showed maxima at 200 nm and 262 nm, consistent with the presence of a pyrimidine moiety³³ (Extended Data Fig. 1).

The ¹H NMR spectrum (600 MHz Bruker spectrometer in DMSO-d₆ at 25°C) revealed one olefinic (H6), five amide (H6', H3, H5, Hα, and Hε-Gln), four methylene (Hβ-Gln, Hγ-Gln, Hα-Gly, and H5'), and five methine (H1', H2', H3', H4', and Hα-Gln) signals (Extended Data Fig. 2a). The 2D ¹H-¹³C-HSQC and -HMBC NMR spectra (600 MHz Bruker spectrometer in DMSO-d₆ at 25°C) identified five carboxyl-amide groups (C2, C4, C=O Gln, C=O Gly, and Cδ-Gln), two olefinic carbons (C1 and C6), four methine carbons belonging to a sugar ring (C1', C2', C3', and C4'), one other methine carbon (Cα-Gln), and four methylene groups (Cα-Gly, Cβ-Gln, Cγ-Gln, and C5') (Extended Data Fig. 2b-c).

The COSY NMR spectrum (600 MHz Bruker spectrometer in DMSO-d₆ at 25°C) identified correlations between the five sugar protons: H1' (δ_H 4.35), H2' (δ_H 3.92), H3' (δ_H 3.65), H4' (δ_H 3.65) and H5' (δ_H -A 3.24; H-B 3.17). The chemical shift of C5' and ribose ¹⁵N-HSQC correlations between H6' and H5' indicated the presence of 6'-amino-ribose. Nitrogen signals N2 and N3 in the ¹⁵N HSQC spectrum, HMBC correlations of H1' to C1, C2 and C6, and HMBC correlations of H6' to C1', C1, C2, and C6, indicated the presence of uracil C-linked to C1' of 6'-amino-ribose. ¹³C-NMR spectra and COSY indicated the presence of a glutaminy moiety, and HMBC correlations of H6' and the methine at δ_H 4.72 (H α -Gln) to the carbonyl at δ_C 169.5 indicated linkage of the glutaminy moiety to N6' of 6'-amino-ribose. N ϵ at δ 108.9 was assigned by ¹⁵N HSQC. The absence of a glutaminy N α signal in the ¹⁵N HSQC spectrum suggested the possible presence of an hydroxamic acid, and this was confirmed by reduction of PUM with aqueous TiCl₃³⁴ to yield desoxy-PUM (**1** in Extended Data Fig. 7a), exhibiting ion-trap ESI-MS mass of 471 [M+H]⁺, ion-trap ESI-MS/MS major peaks at m/z 355 and 372 [M+H]⁺, and a new nitrogen peak at δ 117.7 in the ¹⁵N HSQC spectrum assignable as glutaminy N α , with corresponding NH at δ_H 8.34 coupling with δ_H 4.24 (H α -Gln). The presence of two protons (H α 1 and H β 2) coupling to a HN (δ_N 75) in COSY, the HMBC correlations of H α 1 and H β 2 to a carbonyl at δ_C 157, and a NOESY NMR spectrum (600 MHz Bruker spectrometer in DMSO-d₆ at 25°C) of desoxy-PUM indicated the presence of glycine C-linked to glutamine N α . The chemical shift HN (δ_N 75) with corresponding δ_H 7.43 indicated the presence of formamidine C-linked to glycine N α .

The stereochemistry of the glutamine residue was established to be (L) by total hydrolysis followed by chiral GC-MS (Hewlett-Packard HP5985B GC-MS; procedures as described³⁵). The stereochemistry of the ribose sugar was inferred to be D by analogy to the natural product pseudouridine and was confirmed to be D by comparison of desoxy-PUM prepared by reduction of PUM with TiCl₃ to desoxy-PUM prepared by total synthesis using a D-ribose precursor (Extended Data Fig. 7a-b).

Effects of PUM on macromolecular synthesis

Cultures of *Staphylococcus simulans* strain M22 in 0.5x Mueller Hinton II broth (BD Biosciences) were incubated at 37°C with shaking until OD₆₀₀ = 0.5; diluted in the same medium to OD₆₀₀ = 0.1-0.2; supplemented with 6 kBq/ml [2-¹⁴C]-thymidine (Hartmann Analytic), 40 kBq/ml [5-³H]-uridine (Hartman Analytic), or 6 kBq/ml L-[¹⁴C(U)]-isoleucine (Hartman Analytic); and further incubated at 37°C with shaking. After 15 min, cultures were divided into two equal aliquots, PUM was added to one aliquot to a final concentration of 100-200 μ M, and cultures were further incubated at 37°C with shaking. At time points 0, 10, 20, and 40 min following addition of PUM, 200 μ l aliquots were removed, mixed with 2 ml ice-cold 10% TCA containing 1 M NaCl, and incubated 30-60 min on ice. The resulting TCA precipitates were collected by filtration on glass-microfiber filters (GF/C; Whatman), and filters were washed with 5 ml 2.5% TCA containing 1 M NaCl, transferred to scintillation vials, and dried. Filtersafe scintillation fluid was added (2 ml; Zinnser Analytic), and radioactivity was quantified by scintillation counting (Tri-Carb 3110TR Liquid Scintillation Analyzer; PerkinElmer).

RNAP-inhibitory activity *in vitro*

For experiments in Fig. 1b and Extended Data Table 1 assessing promoter-dependent transcription by *E. coli* RNAP, reaction mixtures contained (25 μ l): 0-20 μ M PUM, 1 U *E. coli* RNAP σ ⁷⁰ holoenzyme (Epicentre), 10 nM DNA fragment carrying positions -112 to -1 of *E. coli* *recA* promoter³⁶ followed by transcribed-region positions +1 to +363 of HeLaScribe Positive Control DNA (Promega; sequence at <https://www.ncbi.nlm.nih.gov/pmc/articles/PMC4021065/bin/1471-2199-15-7-S1.docx>; yields 363 nt transcript), 20 μ M [α ³²P]GTP (0.3 Bq/fmol; PerkinElmer), 400 μ M ATP, 400 μ M CTP, and 6.25 μ M, 50 μ M, or 250 μ M UTP, in 10 mM Tris-HCl (pH. 7.8), 2 mM HEPES-NaOH, 40 mM KCl, 3 mM MgCl₂, 0.2 mM dithiothreitol, 0.09 mM EDTA, 0.2 mM phenylmethylsulfonyl fluoride, and 10% glycerol. Reaction components except RNAP were pre-equilibrated 10 min at 30°C. Reactions were initiated by addition of RNAP, were allowed to proceed 15 min at 30°C, and were terminated by addition of 175 μ l HeLa Extract Stop Solution (Promega). Samples were phenol extracted and ethanol precipitated

(procedures as described³⁷), and pellets were resuspended in 10 μ l 47.5% formamide, 10 mM EDTA, 0.025% bromophenol blue, and 0.01% xylene cyanol and heated 5 min at 95°C. Products were applied to 6% polyacrylamide (19:1 acrylamide:bisacrylamide; 7 M urea)³⁷ slab gels, and gels were electrophoresed in TBE³⁷ at 10 V/cm for 1.5 h, dried using a gel dryer (BioRad)³⁷, and analyzed by storage-phosphor imaging (Typhoon; GE Healthcare).

For experiments in Fig. 1b and Extended Data Table 1 assessing promoter-dependent transcription by human RNAP I, human RNAP II, and human RNAP III, reaction mixtures contained (25 μ l): 0-80 μ M PUM, HeLa nuclear extract [3 μ l HeLa nuclear extract prepared as described³⁸, using $\sim 4 \times 10^7$ HeLa cells grown to 70-80% confluence in DMEM, high glucose, 2 mM L-glutamine medium containing 10% fetal bovine serum (Gibco) and 1% penicillin-streptomycin (Gibco) for assays of human RNAP I; or 6 U HeLaScribe Nuclear Extract (Promega) for assays of human RNAP II and human RNAP III], promoter DNA [4 nM *Eco*RI-linearized plasmid pHrP2x³⁹ carrying human rDNA promoter for assays of human RNAP I (yields 379 nt transcript; 20 nM HeLaScribe Positive Control DNA (Promega) carrying cytomegalovirus immediate early promoter for assays of human RNAP II (yields 363 nt transcript with same sequence as *E. coli*-RNAP-dependent transcript of preceding paragraph); or 2 nM plasmid pVAI⁴⁰ carrying adenovirus VAI promoter for assays of human RNAP III (yields 160 nt transcript)], 20 μ M [α ³²P]GTP (0.3 Bq/fmol; PerkinElmer), 400 μ M ATP, 400 μ M CTP, and 6.25, 50, or 250 μ M UTP, in transcription buffer [12 mM HEPES-NaOH (pH 7.9), 75 mM KCl, 5 mM MgCl₂, 10 mM creatine phosphate, 0.5 mM dithiothreitol, 0.1 mM EDTA, and 12% glycerol, for assays with human RNAP I; 10 mM Tris-HCl (pH 7.8), 2 mM HEPES-NaOH, 44 mM KCl, 3 mM MgCl₂, 0.2 mM dithiothreitol, 0.09 mM EDTA, 0.2 mM phenylmethylsulfonyl fluoride, and 10% glycerol, for assays with human RNAP II and human RNAP III]. Procedures were as in the preceding paragraph.

For experiments in Fig. 1b assessing transcription by *B. subtilis* RNAP, SP6 RNAP, and T7 RNAP, reaction mixtures contained (50 μ l): 0-200 μ M PUM, RNAP [0.2 U nM Rif-resistant *B. subtilis* [469 (513) Gln \rightarrow Arg] β -RNAP σ^A holoenzyme (units defined as described³⁰), 0.2 U SP6 RNAP (Promega), or 0.2 U T7 RNAP (Promega), DNA [0.2 nM plasmid pUC18 (Clontech; for assays with *B. subtilis* RNAP), or 0.2 nM plasmid pGEM-3Z (Promega; for assays with SP6 RNAP and T7 RNAP)], 500 μ M ATP, 500 μ M GTP, 500 μ M CTP, and 6.25 μ M [α ³²P]UTP (0.2 Bq/fmol; PerkinElmer; 6.25, 50, or 250 μ M for Extended Data Table 1), in 40 mM Tris-HCl (pH 7.9), 6 mM MgCl₂, 2 mM spermidine, 10 mM NaCl, 10 mM dithiothreitol, and 10 μ g/ml bovine serum albumin. Reaction components except DNA were pre-equilibrated 15 min at 37°C. Reactions were initiated by addition of DNA, were allowed to proceed 15 min at 37°C, and were terminated by addition of 150 μ l ice-cold 10% (w/v) TCA. After 30 min on ice, the resulting TCA precipitates were collected on glass-fiber filters (UniFilter GF/C; Perkin-Elmer) using a 96-well harvester (Packard). filters were washed once with water, and radioactivity was quantified using a TopCount scintillation counter (Packard).

For experiments in Fig. 1b assessing transcription by ϕ 6 RNA-dependent RNAP, reaction mixtures contained (20 μ l): 0-400 μ M PUM, 0.5 U ϕ 6 RNAP (Thermo Fisher), 2 μ g poly(A) ssRNA (GE Healthcare), 1 μ M poly(U-15) ssRNA primer (Sigma-Aldrich), 400 μ M ATP, 400 μ M GTP, 400 μ M CTP, and 1.56 μ M [α ³²P]UTP (0.02 Bq/fmol; Perkin-Elmer) in 50 mM Tris-acetate (pH 8.7), 50 mM ammonium acetate, and 1.5 mM MnCl₂. Reaction components other than RNA template, RNA primer, and NTPs were pre-incubated 10 min at 30°C. Reactions were initiated by addition of RNA template, RNA primer, and NTPs, reactions were allowed to proceed 1 h min at 30°C, and reactions were terminated by spotting on DE81 filter discs (Whatman; pre-wetted with water) and incubating 1 min at 22°C. Filters were washed with 3x3 ml 0.5 M sodium phosphate dibasic, 2x3 ml water, and 3 ml ethanol using a filter manifold (Hoefer); filters were placed in scintillation vials containing 10 ml Scintiverse BD Cocktail (Thermo Fisher); and radioactivity was quantified by scintillation counting (LS6500; Beckman-Coulter).

For experiments in Extended Data Table 1 assessing promoter-independent transcription by *E. coli* RNAP and HeLa nuclear extract (human RNAP I/II/III), reaction mixtures contained (20 μ l): 0-100 μ M PUM, 100 nM *E. coli* RNAP core enzyme or 8 U HeLaScribe Nuclear Extract (Promega), 1 μ g

human placental DNA (Sigma-Aldrich; catalog number D7011), 400 μ M ATP, 400 μ M GTP, and 400 μ M CTP, and 1.56, 25, or 400 μ M [α^{32} P]UTP (0.1-1 Bq/fmol; PerkinElmer), in 40 mM Tris-HCl (pH 8.0), 7 mM HEPES-NaOH, 70 mM ammonium sulfate, 30 mM KCl, 12 mM MgCl₂, 5 mM dithiothreitol, 0.1 mM EDTA, and 12% glycerol. Procedures were performed as described¹⁸.

For experiments in Extended Data Figs. 4c and 7c, fluorescence-detected transcription assays were performed essentially as described⁵.

Half-maximal inhibitory concentrations (IC₅₀s) were calculated by non-linear regression in SigmaPlot (Systat Software).

Antibacterial activity *in vitro*

Antibacterial activities *in vitro* (Fig. 1c, rows 1-20; Extended Data Fig. 7d) were determined using broth-microdilution growth-curve assays⁴¹ (PUM degrades in phosphate-containing media with a half-life of ~12 h. Broth-microdilution endpoint assays⁴², which have a run time of 16-24 h⁴², which corresponds to 1.3 to 2 PUM half-lives, under-estimate absolute antibacterial activities of PUM. Broth-microdilution growth-curve assays⁴¹, which have shorter run times between assay start and assay signal, more accurately estimate absolute antibacterial activities of PUM.) Colonies of the indicated bacterial strains (5 to 10 per strain) were suspended in 3 ml phosphate-buffered saline³⁷, suspensions were diluted to 1x10⁵ cfu/ml with growth medium [Todd Hewitt broth (BD Biosciences) for *Streptococcus pyogenes* and *Streptococcus pneumoniae*, aged Mueller Hinton II cation-adjusted broth (BD Biosciences; autoclaved and allowed to stand 2-12 months at room temperature before use) for *Staphylococcus aureus* and *Enterococcus faecium*, fresh Mueller Hinton II cation-adjusted broth (autoclaved and used immediately) for *Moraxella catarrhalis*, or fresh Mueller Hinton II cation-adjusted broth (BD Biosciences; autoclaved and used immediately) containing 0.4% *Haemophilus* Test Medium⁴³ and 0.5% yeast extract for *Haemophilus influenzae*], 50 μ l aliquots were dispensed into wells of a 96-well microplate containing 50 μ l of the same medium or 50 μ l of a 2-fold dilution series of PUM in the same medium (final concentrations = 0 and 0.25-256 μ M), plates were incubated at 37°C with shaking, and optical densities at 600 nm were recorded at least hourly using a Synergy 2 (BioTek) or GENios Pro (Tecan) microplate reader. For each dilution series, growth curves were plotted, areas under growth curves were calculated, and IC₅₀ was extracted as the lowest tested concentration of PUM that reduced area under the growth curve to 50% that in the absence of PUM (using only time points for rise phase of the growth curve in the absence of PUM).

Identical results were obtained in assays in the absence and presence of 30% human serum (Sigma-Aldrich; Fig. 1c, rows 1-4), indicating that PUM does not bind tightly to human serum proteins (unbound fraction ~100%).

Cytotoxicities for human macrovascular endothelial cells and human monocytes in culture (Fig. 1c, rows 21-22) were determined as described⁴⁴.

Antibacterial activity *in vivo*

Antibacterial activity *in vivo* was assessed in a mouse *S. pyogenes* peritonitis model (Fig. 1d; Extended Data Table 2). Female ICR mice (weight = 23-25 g; Harlan Laboratories Italy) were adapted to standardized environmental conditions (temperature = 23 \pm 2°C; humidity = 55% \pm 10%) for one week prior to infection. Infection was induced by intraperitoneal injection of 0.5 ml saline solution (supplemented with 1% peptone) containing 4 x 10³ cfu *S. pyogenes* C203 (an inoculum resulting in \geq 95% mortality in untreated controls within 48 to 72 h after infection). Infected mice (eight mice per group; number determined by power calculations; assigned randomly to groups; unblinded) were treated with either: (i) 0.2 ml 5% dextrose or 0.2 ml of a 2.5-fold dilution series of PUM in 5% dextrose, administered intravenously 10 min after infection and again 6 h after infection (total PUM dose = 0 or 3.2-50 mg/kg), (ii) 0.25 ml 5% dextrose or 0.25 ml of a 2.5-fold dilution series of PUM in 5% dextrose, administered intravenously 10 min after infection (total PUM dose = 0 or 1.024-40 mg/kg), or (iii) 0.25 ml 5% dextrose or 0.25 ml of a 2.5-fold dilution series of PUM in 5% dextrose, administered

subcutaneously 10 min after infection (total PUM dose = 0 or 1.024-40 mg/kg). Survival was monitored for 7 days after infection. Experiments were performed in compliance with vertebrate animal ethical regulations and with Institutional Animal Care and Use Committee (IACUC) approval.

ED50s (doses yielding 50% survival at 7 days) and 95% confidence limits were calculated using the trimmed Spearman-Kärber method as implemented in the US EPA LC50 Model System (<http://sdi.odu.edu/model/lc50.php>)⁴⁵.

Checkerboard interaction assays

Antibacterial activities of combinations of PUM and Rif were assessed in checkerboard interaction assays⁴⁶⁻⁴⁷ (Fig. 1e). Broth-macrodilution (assays procedures essentially as described⁴²) were performed in checkerboard format, using *S. pyogenes* strain L49 or *S. pneumoniae* strain L44, and using Todd Hewitt broth (BD Biosciences) containing pairwise combinations of: (i) PUM at 1x, 0.5x, 0.25x, 0.125x, 0.063x, 0.031x, 0.016x, and 0.0078x MIC_{PUM} and (ii) Rif at 0.8x, 0.4x, 0.2x, 0.1x, 0.05x, 0.025x, and 0.0125x MIC_{Rif}. Fractional inhibitory concentrations (FICs), FIC indices (FICIs), and minimum and maximum FICIs (FICI_{min} and FICI_{max}) were calculated as described⁴⁷. FICI_{min} ≤ 0.5 was deemed indicative of super-additivity (synergism), FICI_{min} > 0.5 and FICI_{max} ≤ 4.0 was deemed indicative of additivity, and FICI_{max} > 4.0 was deemed indicative of sub-additivity (antagonism)⁴⁶⁻⁴⁷.

Spontaneous resistance rate assays

Spontaneous resistance rates were determined in Luria-Delbrück fluctuation assays⁴⁸ (Fig. 2a). *S. pyogenes* strain ATCC 12344 (~1 x 10⁹ cfu/plate) was plated on Todd Hewitt agar [Todd Hewitt broth (BD Biosciences) supplemented with 1.5% Bacto agar (BD Biosciences)] containing 64 µg/ml or 128 µg/ml PUM (8x or 16x MIC under these conditions) or 1 µg/ml or 2 µg/ml Rif (8x or 16x MIC under these conditions), and numbers of colonies were counted after 24 h at 37°C (at least six independent determinations each). Resistance rates and 95% confidence intervals were calculated using the Ma-Sandri-Sarkar Maximum Likelihood Estimator⁴⁹⁻⁵⁰ as implemented on the Fluctuation Analysis Calculator (<http://www.keshavsingh.org/protocols/FALCOR.html>)⁵¹.

Spontaneous PUM-resistant mutants, *S. pyogenes*.

To isolate spontaneous PUM-resistant mutants of *S. pyogenes* (Fig. 2b), a single colony of *S. pyogenes* ATCC 12344 was inoculated into 5 ml Todd Hewitt broth (BD Biosciences) and incubated 3 h at 37°C with shaking in a 7% CO₂/6% O₂/4% H₂/83% N₂ atmosphere (atmosphere controlled using Anoxomat AN2CTS; Advanced Instruments), the culture was centrifuged, and the cell pellet (~1 x 10⁹ cells) was re-suspended in 50 µl Todd Hewitt broth and plated on Todd Hewitt agar (BD Biosciences) containing 16-256 µg/ml PUM (2-32x MIC under these conditions), and plates were incubated 120 h at 37°C in a 7% CO₂/6% O₂/4% H₂/83% N₂ atmosphere. PUM-resistant mutants were identified by the ability to form colonies on these media, were confirmed to be PUM-resistant by re-streaking on the same media, and were confirmed to be *S. pyogenes*, (as opposed to contaminants) using Taxo A differentiation discs (BD Biosciences) and Pyrase strips (Fluka).

Genomic DNA was isolated using the Wizard Genomic DNA Purification Kit [Promega; procedures as specified by the manufacturer, but with cells lysed using 1 mg/ml lysozyme (Sigma-Aldrich)] and was quantified by measurement of UV-absorbance (procedures as described³⁷). The *rpoC* gene and the *rpoB* gene were PCR-amplified in reactions containing 0.2 µg genomic DNA, 0.4 µM forward and reverse oligodeoxynucleotide primers (5'-GGGCAAATGATAACTTAGTTGCGATTTGCTG-3' and 5'-CCTTTCTGCCTTTGATGACTTTACCAGTTC-3' for *rpoB*; 5'-GCTCAAGAACTCAAGAAGTTTCTGAAACAACGAC-3' and 5'-GTCAATGCTTTTTACTGCCAACAACTCAGAC-3' for *rpoC*), 5 U Taq DNA polymerase (Genscript), and 800 µM dNTP mix (200 µM each dNTP; Agilent/Stratagene) (initial denaturation step of 3 min at 94°C; 30 cycles of 30 s at 94°C, 45 s at 53°C, and 4 min at 68°C; final extension step of 10 min

at 68°C). PCR products containing the *rpoC* gene (3.6 kB) or the *rpoB* gene (3.6 kB) were isolated by electrophoresis on 0.8% agarose gels (procedures as described³⁷), extracted from gel slices using a Gel/PCR DNA Fragments Extraction Kit (IBI Scientific; procedures as specified by the manufacturer), and sequenced (GENEWIZ; Sanger sequencing; seven sequencing primers per gene).

Spontaneous PUM-resistant mutants, *E. coli*

To isolate spontaneous PUM-resistant mutants of *E. coli* (Extended Data Fig. 4a), *E. coli* uptake-proficient, efflux-deficient strain D21f2tolC⁵² was cultured to saturation in 10 ml LB broth³⁷ at 37°C, cultures were centrifuged, cell pellets (~1 x 10¹⁰ cells) were re-suspended in 50 µl LB broth and plated on LB agar³⁷ containing 800 µg/ml PUM (~1x MIC under these conditions), and plates were incubated 96-120 h at 37°C. PUM-resistant mutants were identified by the ability to form colonies on this medium.

Genomic DNA was isolated, and *rpoB* and *rpoC* genes were PCR-amplified and sequenced as described¹⁸.

Resistance and cross-resistance levels

Resistance levels of *S. pyogenes* and *E. coli* spontaneous PUM-resistant mutants (Fig. 2b Extended Data Fig. 4b) were quantified in broth-microdilution assays. A single colony of a mutant strain or the isogenic wild-type parent strain was inoculated into 5 ml Todd Hewitt broth (BD Biosciences; for *S. pyogenes*) or LB broth³⁷ (for *E. coli*) and incubated at 37°C with shaking in a 7% CO₂/6% O₂/4% H₂/83% N₂ atmosphere (atmosphere controlled using Anoxomat AN2CTS; Advanced Instruments); for *S. pyogenes*) or in air (for *E. coli*) until OD₆₀₀ = 0.4-0.8. Diluted aliquots (~2 x 10⁵ cells in 50 µl same medium) were dispensed into wells of a 96-well microplate containing 50 µl of the same medium or 50 µl of a 2-fold dilution series of PUM in the same medium (final PUM concentration = 0 or 0.098-800 µg/ml), and were incubated 16 h at 37°C with shaking in a 7% CO₂/6% O₂/4% H₂/83% N₂ atmosphere (for *S. pyogenes*) or in air (for *E. coli*). MIC was defined as the lowest tested concentration of PUM that inhibited bacterial growth by ≥90%. MIC/MIC_{wild-type} was defined as the ratio of MIC for mutant to MIC for isogenic wild-type parent (*S. pyogenes* MIC_{wild-type} = 6.25 µg/ml under these conditions; *E. coli* MIC_{wild-type} = 400 µg/ml under these conditions).

Cross-resistance levels of *S. pyogenes* and *E. coli* spontaneous PUM-resistant mutants (Fig. 2e; Extended Data Fig. 4f) were determined as in the preceding paragraph, but using culture aliquots (~1x10⁵ cells) in 97 µl growth medium supplemented with 3 µl methanol or 3 µl of a 2-fold dilution series of Rif (Sigma-Aldrich; *S. pyogenes* MIC_{wild-type} = 0.098 µg/ml; *E. coli* MIC_{wild-type} = 0.20 µg/ml), lipiarmycin A3 (Lpm; BioAustralis; *S. pyogenes* MIC_{wild-type} = 6.25 µg/ml; *E. coli* MIC_{wild-type} = 1.56 µg/ml), myxopyronin B (Myx; prepared as described⁵³; *S. pyogenes* MIC_{wild-type} = 6.25 µg/ml; *E. coli* MIC_{wild-type} = 0.20 µg/ml), streptolydigin (Stl; Sourcon-Padena; *S. pyogenes* MIC_{wild-type} = 3.13 µg/ml; *E. coli* MIC_{wild-type} = 3.13 µg/ml), CBR703 (CBR; Maybridge; *E. coli* MIC_{wild-type} = 6.25 µg/ml), or salinamide A (Sal; W. Fenical, Scripps Institution of Oceanography; *E. coli* MIC_{wild-type} = 0.049 µg/ml) in methanol (final concentrations = 0 and 0.006-50 µg/ml), or using culture aliquots (~2x10⁵ cells) in 50 µl growth medium supplemented with 50 µl growth medium or 50 µl of a 2-fold dilution series of GE23077 (GE; prepared as described⁵⁴; *E. coli* MIC_{wild-type} = 500 µg/ml) in growth medium (final concentrations = 0 and 125-8000 µg/ml).

Cross-resistance levels of *S. pyogenes* Rif-resistant mutants to PUM (Fig. 1e) were determined were determined as described for cross-resistance levels of *S. pyogenes* spontaneous PUM-resistant mutants, but analyzing a collection of 13 *S. pyogenes* spontaneous Rif-resistant mutants [isolated and sequenced using the same procedures used for isolation and sequencing of *S. pyogenes* PUM-resistant mutants (Methods, Spontaneous PUM-resistant mutants, *S. pyogenes*), but using Todd Hewitt agar containing 1-16x MIC Rif (0.1-2 µg/ml under these conditions)] and the isogenic wild-type parent, and analyzing a 2-fold dilution series of PUM (final concentration = 0 or 1.56-100 µg/ml).

Cross-resistance levels of *E. coli* Rif-, Lpm-, Myx-, and Sal-resistant mutants to PUM (Extended Data Fig. 4g-i,l) were determined as described for resistance levels of *E. coli* spontaneous PUM-resistant mutants, but analyzing a collection of *E. coli* D21f2tolC derivatives¹⁸ comprising four chromosomal Rif-

resistant mutants, five chromosomal Lpm-resistant mutants, five chromosomal Myx-resistant mutants, five chromosomal Sal-resistant mutants, and the isogenic wild-type parent, and analyzing a 2-fold dilution series of PUM (final concentration = 0 or 25-1600 µg/ml).

Cross-resistance levels of *E. coli* Stl-, CBR-, and GE-resistant mutants to PUM (Extended Data Fig. 4j-k,n) were determined analogously, analyzing a collection of *E. coli* D21f2tolC pRL706 and *E. coli* D21f2tolC pRL663 derivatives^{5,14,16} comprising five plasmid-based Stl-resistant mutants, five plasmid-based CBR-resistant mutants, six plasmid-based GE-resistant mutants, and plasmid-based wild-type isogenic parents. Single colonies were inoculated into 5 ml LB broth containing 200 µg/ml ampicillin (Sigma-Aldrich), incubated at 37°C with shaking until OD₆₀₀ = 0.4-0.8, supplemented with IPTG (Gold Bio) to a final concentration of 1 mM, and further incubated 1 h at 37°C with shaking. Diluted aliquots (~2 x 10⁵ cells in 50 µl LB broth containing 200 µg/ml ampicillin and 1 mM IPTG) were dispensed into wells of a 96-well microplate containing 50 µl of the same medium or 50 µl of a 2-fold dilution series of PUM in the same medium (final concentration = 0 or 25-4000 µg/ml), and were incubated 16 h at 37°C with shaking.

Amino-acid substitutions that confer PUM-resistance in the context of *S. pyogenes* RNAP were re-constructed and re-analyzed in the context of *E. coli* RNAP using an *E. coli* plasmid-based resistance assay (Extended Data Fig. 4b). Site-directed mutagenesis (QuikChange Site-Directed Mutagenesis Kit; Agilent) was used to construct plasmid pRL706²⁸ and pRL663⁵⁵ derivatives encoding *E. coli* RNAP β-subunit and β'-subunit derivatives having amino-acid substitutions that confer PUM-resistance in *S. pyogenes* (sequences from Fig. 2b). The resulting plasmids were introduced by transformation into *E. coli* strain D21f2tolC⁵², and resistance levels of transformants were determined using the procedures of the preceding paragraph.

Formation of RNAP-promoter open complex

Experiments (Extended Data Fig. 4a) were performed essentially as described¹². Reaction mixtures contained (20 µl): test compound (0 or 500 µM PUM, 2 µM Rif, or 100 µM Lpm), 40 nM *E. coli* RNAP σ⁷⁰ holoenzyme, 10 nM Cy5-labelled DNA fragment carrying positions -40 to +15 of *lacUV5* promoter (*lacUV5*[-40;+15]-Cy5¹²), and 100 µg/ml heparin, in 50 mM Tris-HCl (pH 8.0), 100 mM KCl, 10 mM MgCl₂, 1 mM dithiothreitol, 10 µg/ml bovine serum albumin, and 5% glycerol. Reaction components other than DNA and heparin were incubated 10 min at 37°C; DNA was added and reactions were incubated 15 min at 37°C; and heparin was added and reactions were incubated 2 min at 37°C. Products were applied to 5% TBE-polyacrylamide slab gels (Bio-Rad), electrophoresed in TBE³⁷, and analyzed by fluorescence scanning (Typhoon 9400).

Nucleotide addition in transcription initiation.

Experiments were performed essentially as described⁵, using reaction mixtures that contained no inhibitor, 500 µM PUM, 2 µM Rif, or 100 µM Lpm, and using 5 µM [α³²P]UTP (3 Bq/fmol; PerkinElmer) (Extended Data Fig. 4b).

Nucleotide addition in transcription elongation

Experiments were performed essentially as described⁵, using reaction mixtures that contained no inhibitor, 500 µM PUM, 2 µM Rif, or 100 µM Lpm (Extended Data Fig. 4c).

Nucleotide addition at elevated NTP concentrations

Experiments (Fig. 3a) were performed essentially as described above for assays of promoter-dependent transcription by *B. subtilis* RNAP (Methods, RNAP-inhibitory activity *in vitro*), using reaction mixtures (50 µl) that contained 0 or 6 µM PUM, 0.4 U *E. coli* RNAP σ⁷⁰ holoenzyme (Epicentre), 0.4 nM plasmid pUC19 Clontech), 80 mM HEPES-KOH (pH 7.5), 80 mM KCl, 4 mM MgCl₂, 0.1 mM EDTA, 5 mM dithiothreitol, 100 µg/ml bovine serum albumin, and either (i) 100 µM ATP, 100 µM [α³²P]CTP (0.2 Bq/fmol; PerkinElmer), 100 µM GTP, and 10-500 µM UTP; (ii) 10-500

μM GTP, 100 μM ATP, 100 μM CTP, and 2 μM [$\alpha^{32}\text{P}$]UTP (0.2 Bq/fmol; PerkinElmer); (iii) 100 μM GTP, 10-500 μM A, 100 μM CTP, and 2 μM [$\alpha^{32}\text{P}$]UTP (0.2 Bq/fmol); or (iv) 100 μM GTP, 100 μM ATP, 10-500 μM CTP, and 2 μM [$\alpha^{32}\text{P}$]UTP (0.2 Bq/fmol). The reaction time was 30 min at 37°C. Relative nucleotide incorporation was defined as the ratio of nucleotide incorporation in the presence of PUM to nucleotide incorporation in the absence of PUM.

Nucleotide addition on standard and "U-less cassette" templates

Experiments (Fig. 3b) were performed essentially as described in the preceding section (Methods, Nucleotide addition at elevated NTP concentrations), using reaction mixtures (50 μl) that contained 0-20 μM PUM, 0.4 U *E. coli* RNAP σ^{70} holoenzyme (Epicentre), 2 μM [$\alpha^{32}\text{P}$]CTP (0.2 Bq/fmol; PerkinElmer), 100 μM ATP, 100 μM GTP, and 5 μM UTP, in 40 mM Tris-HCl (pH 7.5), 10 mM MgCl_2 , 5 mM dithiothreitol, 15 mM KCl, 0.01 % Triton X-100, and 100 $\mu\text{g/ml}$ bovine serum albumin, and either (i) 50 nM DNA fragment carrying positions -112 to +8 of *E. coli* *recA* promoter³⁶ followed by 5'-CAGGGACAAGTTAGTTCGTTTCAGCGACACGCGGCAACAAG-3' (directs incorporation of U, G, A, and C) or (ii) 50 nM DNA fragment carrying positions -112 to +8 of *E. coli* *recA* promoter followed by 5'-CAGGGACAAGGAGACCAACGCAGCGACACGCGGCAACAAG-3' ("U-less cassette"; directs incorporation of G, A, and C).). The reaction time was 60 min at 37°C. Relative nucleotide incorporation was defined as the ratio of nucleotide incorporation in the presence of PUM to nucleotide incorporation in the absence of PUM.

Template-sequence specificity of inhibition by PUM: single-nucleotide-addition reactions

Template-sequence specificity of inhibition by PUM was assessed in single-nucleotide-addition experiments (Fig. 3c) using *E. coli* RNAP transcription elongation complexes assembled on the following nucleic-acid scaffolds (black, DNA; red, RNA; asterisk, ^{32}P):

```
incoming NTP = UTP; RNA 3' end = G
      5'-ACGCCAGACAGGG-3'
      3'-GCCGCGCGCATGCGGTCTGTCCC-5'
      5'-*CGGCGCGCG-3'
```

```
incoming NTP = GTP; RNA 3' end = G
      5'-ACGCCAGACAGGG-3'
      3'-GCCGCGCGCCTGCGGTCTGTCCC-5'
      5'-*CGGCGCGCG-3'
```

```
incoming NTP = ATP; RNA 3' end = G
      5'-tCGCCAGACAGGG-3'
      3'-GCCGCGCGCTaGCGGTCTGTCCC-5'
      5'-*CGGCGCGCG-3'
```

```
incoming NTP = CTP; RNA 3' end = G
      5'-ACGCCAGACAGGG-3'
      3'-GCCGCGCGGTGCGGTCTGTCCC-5'
      5'-*CGGCGCGCG-3'
```

```
incoming NTP = UTP; RNA 3' end = A
      5'-ACGCCAGACAGGG-3'
      3'-GCCGCGCGTATGCGGTCTGTCCC-5'
      5'-*CGGCGCGCA-3'
```

```
incoming NTP = GTP; RNA 3' end = A
      5'-ACGCCAGACAGGG-3'
      3'-GCCGCGCGTCTGCGGTCTGTCCC-5'
      5'-*CGGCGCGCA-3'
```

```
incoming NTP = ATP; RNA 3' end = A
      5'-tCGCCAGACAGGG-3'
```

```

3'-GCCGCGCGTTaGCGGTCTGTCCC-5'
5'-*CGGCGCGCA-3'

incoming NTP = CTP; RNA 3' end = A
5'-ACGCCAGACAGGG-3'
3'-GCCGCGCGTGTGCGGTCTGTCCC-5'
5'-*CGGCGCGCA-3'

incoming NTP = UTP; RNA 3' end = U
5'-ACGCCAGACAGGG-3'
3'-GCCGCGCGAATGCGGTCTGTCCC-5'
5'-*CGGCGCGCU-3'

incoming NTP = GTP; RNA 3' end = U
5'-ACGCCAGACAGGG-3'
3'-GCCGCGCGACTGCGGTCTGTCCC-5'
5'-*CGGCGCGCU-3'

incoming NTP = ATP; RNA 3' end = U
5'-tCGCCAGACAGGG-3'
3'-GCCGCGCGATaGCGGTCTGTCCC-5'
5'-*CGGCGCGCU-3'

incoming NTP = CTP; RNA 3' end = U
5'-ACGCCAGACAGGG-3'
3'-GCCGCGCGAGTGCGGTCTGTCCC-5'
5'-*CGGCGCGCU-3'

incoming NTP = UTP; RNA 3' end = C
5'-ACGCCAGACAGGG-3'
3'-GCCGCGCGGATGCGGTCTGTCCC-5'
5'-*CGGCGCGCC-3'

incoming NTP = GTP; RNA 3' end = C
5'-ACGCCAGACAGGG-3'
3'-GCCGCGCGGTGCGGTCTGTCCC-5'
5'-*CGGCGCGCC-3'

incoming NTP = ATP; RNA 3' end = C
5'-tCGCCAGACAGGG-3'
3'-GCCGCGCGGTaGCGGTCTGTCCC-5'
5'-*CGGCGCGCC-3'

incoming NTP = CTP; RNA 3' end = C
5'-ACGCCAGACAGGG-3'
3'-GCCGCGCGGGTGCGGTCTGTCCC-5'
5'-*CGGCGCGCC-3'

```

Nucleic-acid scaffolds for single-nucleotide-addition reactions were prepared as follows: 1 μ M nontemplate-strand oligodeoxyribonucleotide [5'-ACGCCAGACAGGG-3' or 5'-TCGCCAGACAGGG-3'; IDT], 1 μ M template-strand oligodeoxyribonucleotide [5'-GCCGCGCG-(C or T or A or G)-(A or C or G)-TGCGGTCTGTCCC-5' or 5'-GCCGCGCG-(C or T or A or G)-(T)-AGCGGTCTGTCCC-5'; IDT], and 1 μ M 32 P-5'-end-labeled oligoribonucleotide [5'- 32 P-CGGCGCGC-(U or C or A or G)-3'; 90 Bq/fmol; prepared using T4 polynucleotide kinase (New England Biolabs), [γ - 32 P]ATP (100 Bq/fmol; PerkinElmer), and corresponding unlabelled oligoribonucleotide (IDT); procedures as described³⁷], in 5 mM Tris-HCl (pH 7.7), 200 mM NaCl, and 10 mM MgCl₂, were heated 5 min at 95°C, cooled to 4°C in 2°C steps with 1 min/step using a thermal cycler (Applied Biosystems), and stored at -20°C. Reaction mixtures for single-nucleotide-addition reactions contained (10 μ l): 0 or 25 μ M PUM, 40 nM *E. coli* RNAP core enzyme, 10 nM nucleic-acid scaffold, and 2.5 μ M ATP, GTP, CTP, or UTP, in 50 mM Tris-HCl (pH 8.0),

100 mM KCl, 10 mM MgCl₂, 1 mM dithiothreitol, 10 µg/ml BSA, and 5% glycerol. Reaction components except PUM and NTP were pre-incubated 10 min at 37°C, PUM was added and reaction mixtures were incubated 5 min at 37°C, and NTP was added and reaction mixtures were incubated 5 min at 37°C. Reactions were terminated by addition of 5 µl 80% formamide, 10 mM EDTA, 0.04% bromophenol blue, 0.04% xylene cyanol, and 0.08% amaranth red, and heating 2 min at 95°C. Samples were applied to denaturing 15% polyacrylamide (19:1 acrylamide:bisacrylamide, 7 M urea)³⁷ slab gels, electrophoresed in TBE³⁷, and analyzed by storage-phosphor scanning (Typhoon 9400; GE Healthcare).

Template-sequence specificity of inhibition by PUM: multiple-nucleotide-addition reactions

Template-sequence specificity of inhibition by PUM was assessed in multiple-nucleotide-addition experiments (Fig. 3d), performed by adding PUM to transcription elongation complexes halted at position +29 of a 100 bp transcription unit by omission of CTP, re-starting transcription elongation complexes and allowing transcription of positions +30 to +100 of the transcription unit by addition of CTP, and identifying positions at which PUM inhibits transcription.

Halted transcription elongation complexes were prepared as described⁵⁶. Reaction mixtures (20 µl) contained: 40 nM *E. coli* RNAP σ^{70} holoenzyme, 10 nM DNA fragment N25-100-tR2⁵⁶, 100 µg/ml heparin, 5 µM [γ^{32} P]ATP (6 Bq/fmol; PerkinElmer), 5 µM UTP, and 5 µM GTP, in 50 mM Tris-HCl (pH 8.0), 100 mM KCl, 10 mM MgCl₂, 1 mM dithiothreitol, 10 µg/ml bovine serum albumin, and 5% glycerol. Reaction components other than heparin and NTPs were pre-incubated 5 min at 30°C; heparin was added and reaction mixtures were incubated 2 min at 30°C; NTPs were added and reaction mixtures were incubated 3 min at 30°C. Halted transcription elongation complexes were provided with PUM (1.25 µl 125 µM PUM, 1.25 µl 250 µM PUM, 1.25 µl 500 µM PUM, or 1.25 µl 1 mM PUM) or, to provide markers, chain-terminating 3'-O-methyl-NTPs (RiboMed; 1.25 µl 400 µM 3'-O-methyl-UTP, 1.25 µl 400 µM 3'-O-methyl-CTP, 1.25 µl 400 µM 3'-O-methyl-GTP, or 1.25 µl 400 µM 3'-O-methyl-ATP), were incubated 3 min at 30°C, were re-started by addition of 0.625 µl 200 µM UTP, 1.25 µl 200 µM CTP, 0.625 µl 200 µM GTP, and 0.625 µl 200 µM ATP, and were further incubated 10 min at 30°C. Reactions were terminated by addition of 12.5 µl 80% formamide, 10 mM EDTA, 0.04% bromophenol blue, 0.04% xylene cyanol, and 0.08% amaranth red, and heating 4 min at 95°C. Samples were applied to 10% polyacrylamide (19:1 acrylamide:bisacrylamide; 7 M urea)³⁷ slab gels, electrophoresed in TBE³⁷, and analyzed by storage-phosphor scanning (Typhoon 9400).

Structure determination: RPo-GpA-PUM

Crystals of *T. thermophilus* RPo-GpA were prepared as described²⁶. Crystallization drops contained 1 µl 18 µM RPo (prepared from *T. thermophilus* RNAP σ^A holoenzyme and synthetic nucleic-acid scaffold as described²⁶) and 1 mM GpA (RiboMed) in 20 mM Tris-HCl, pH 7.7, 100 mM NaCl, and 1% glycerol, and 1 µl reservoir buffer (RB; 100 mM Tris-HCl, pH 8.4, 200 mM KCl, 50 mM MgCl₂, and 10% PEG4000), and were equilibrated against 400 µl RB in a vapor-diffusion hanging-drop tray (Hampton Research). Rod-like crystals appeared in 1 day, and grew to a final size of 0.1 mm x 0.1 mm x 0.3 mm in 5 days.

PUM was soaked into RPo-GpA crystals by adding 0.2 µl 100 mM PUM in RB to the crystallization drop and incubating 30 min at 22°C. RPo-GpA-PUM crystals were transferred to reservoir solutions containing 2 mM PUM in 17.5% (v/v) (2R,3R)-(-)-2,3-butanediol (Sigma-Aldrich) and were flash-cooled with liquid nitrogen.

Diffraction data for RPo-GpA-PUM were collected from cryo-cooled crystals at Cornell High Energy Synchrotron Source (CHESS) beamline F1. Data were integrated and scaled using HKL2000⁵⁷. Structure factors were converted using the French-Wilson algorithm in Phenix⁵⁸ and were subjected to anisotropy correction using the UCLA MBI Diffraction Anisotropy server (<http://services.mbi.ucla.edu/anisotropy/>)⁵⁹.

The structure of RPo-GpA-PUM was solved by molecular replacement in Molrep⁶⁰, using one RNAP molecule from the structure of *T. thermophilus* RPo (PDB 4G7H²⁶) as the search model.

Early-stage refinement included rigid-body refinement of each RNAP molecule, followed by rigid-body refinement of each subunit of each RNAP molecule. Cycles of iterative model building with Coot⁶¹ and refinement with Phenix⁶² were performed. Atomic models of the DNA nontemplate strand, the DNA template strand, and GpA were built into mFo-DFc omit maps, and further refinement with Phenix was performed. The atomic model of PUM was built into the mFo-DFc omit map and was refined with Phenix. The final crystallographic model of RPo-GpA-PUM at 3.30 Å resolution, refined to Rwork and Rfree of 0.232 and 0.280, has been deposited in the PDB with accession code 5X21 (Fig. 4a; Extended Data Table 3).

Structure determination: RPo-GpA-CMPcPP

Crystals of *T. thermophilus* RPo-GpA-CMPcPP were prepared by co-crystallization. Crystallization drops contained 1 µl 18 µM RPo (prepared from *T. thermophilus* RNAP σ^A holoenzyme and synthetic nucleic-acid scaffold as described²⁶), 1 mM GpA (RiboMed), and 10 mM CMPcPP (Jena Bioscience) in 20 mM Tris-HCl, pH 7.7, 100 mM NaCl, and 1% glycerol, and 1 µl RB, and were equilibrated against 400 µl RB in a vapor-diffusion hanging-drop tray (Hampton Research). Rod-like crystals appeared in 1 day, and grew to a final size of 0.1 mm x 0.1 mm x 0.3 mm in 5 days. RPo-GpA-CMPcPP crystals were transferred to reservoir solutions containing 2 mM CMPcPP in 17.5% (v/v) (2R,3R)-(-)-2,3-butanediol (Sigma-Aldrich), and were flash-cooled with liquid nitrogen.

Diffraction data for RPo-GpA-CMPcPP were collected from cryo-cooled crystals at CHESS beamline F1. Data were integrated and scaled, structure factors were converted and subjected to anisotropy correction, and the structure was solved and refined using procedures analogous to those in the preceding section. The final crystallographic model of RPo-GpA-CMPcPP at 3.35 Å resolution, refined to Rwork and Rfree of 0.208 and 0.250, has been deposited in the PDB with accession code 5X22 (Fig. 4b; Extended Data Table 3).

Semi-synthesis of PUM derivatives

Semi-syntheses of PUM derivatives from PUM corroborate the inferred structure of PUM, provide routes for preparation of novel PUM derivatives, and provide initial structure-activity relationships (Extended Data Fig. 7a,c-d). Reactions were conducted starting from 1 mg PUM, and products were identified by LC-MS (Agilent 1100 with flow split in 1:1 ratio between UV detector and ion-trap ESI-MS interface of Bruker Esquire 3000 Plus; Waters Atlantis 3 µm, 50 x 4.6 mm, column; phase A = 0.05% trifluoroacetic acid in water; phase B = acetonitrile; gradient = 5-95% B in 6 min; flow rate = 1 ml/min; run temperature = 40°C; PUM retention time = 1.4 min).

Reaction of PUM with TiCl₃ in 1 M sodium acetate (pH 7.0) for 2 h at room temperature resulted in reduction of the N-hydroxy moiety, yielding desoxy-PUM (**1**; $m/z = 471$ [M+H]⁺). Reaction of PUM with PdCl₂⁶³ in 1:1 acetonitrile:water for 2 h at room temperature resulted in selective dehydration of the PUM glutamine sidechain amide -NH₂, yielding nitrile analog **2** ($m/z = 469$ [M+H]⁺). Reaction of PUM with 0.1% TFA in water for 3 days at room temperature resulted in hydrolysis of the glutamine sidechain amide, yielding carboxy analog **3** ($m/z = 488$ [M+H]⁺). Reaction of **3** with benzylamine in DMF containing benzotriazol-1-yl-oxytripyrrolidinophosphonium hexafluorophosphate (PyBOP) for 30 min at room temperature yielded benzylamide analog **4** ($m/z = 577$ [M+H]⁺). Reaction of PUM with 2,3-butanedione⁶⁴ in 10 mM ammonium acetate (pH 8.0) for 30 min at room temperature resulted in diolic intermediate **5** ($m/z = 573$ [M+H]⁺), which subsequently was trapped by treatment with phenylboronic acid for 2 h at room temperature, yielding phenyl-dioxaborolan analog **6** ($m/z = 659$ [M+H]⁺).

Total synthesis of desoxy-PUM

Total synthesis of desoxy-PUM provides a reference compound that corroborates the inferred stereochemistry of PUM [by comparison of desoxy-PUM prepared by total synthesis (**1** in Extended Data Fig. 7b) to desoxy-PUM prepared by semi-synthesis from PUM (**1** in Extended Data Fig. 7a) and provides an additional route to novel PUM derivatives. Desoxy-PUM was obtained in eight steps by

convergent synthesis from commercially available β -D-pseudouridine and glycyl-L-glutamine, as follows (Extended data Fig. 7b):

Acetonide protection (reaction a in Extended Data Fig. 7b). To a solution of β -D-pseudouridine (Berry & Associates; 400 mg, 1.64 mmol) and 2,2-dimethoxypropane (Sigma-Aldrich; 12 ml) in dimethylformamide (8 ml), concentrated HCl (80 μ L) was added, and the reaction mixture was stirred 5 h at room temperature. After neutralization with 2.5 M NaOH, solvent was removed under vacuum. ^1H -NMR (400 MHz, D_2O , δ -H): 1.35 (s, 3H, CH_3), 1.56 (s, 3H, CH_3), 3.67 (dd, 1H, $J = 12.2, 5.65$ Hz, H-5'), 3.75 (dd, 1H, $J = 12.2, 3.75$ Hz, H-5'), 4.11 (dd, 1H, H-4'), 4.75 (m, 2H), 4.86 (m, 1H), 7.62 (s, 1H, H-6).

Mesylation (reaction b in Extended Data Fig. 7b). To a solution of the crude product of the preceding step (419 mg, 1.47 mmol) in pyridine (Sigma-Aldrich; 4.7 ml), methanesulfonyl chloride (Sigma-Aldrich; 95 μ L, 1.23 mmol) was added with stirring at 0°C . The reaction mixture was stirred at room temperature until completeness (16 h). Solvent was removed by rotary evaporation, and the raw material was purified by flash chromatography on Combiflash (Teledyne ISCO), yielding 475 mg of a white powder (95% yield). ^1H -NMR (400 MHz, acetonitrile- d_3 , δ -H): 1.32 (s, 3H, CH_3), 1.54 (s, 3H, CH_3), 4.33 (dd, 1H, $J = 11$ Hz, H-5'), 4.46 (dd, 1H, $J = 11$ Hz, H-5'), 4.20 (m, 1H), 4.72 (dd, 1H), 4.80 (m, 2H), 7.55 (s, 1H, H-6), 10.23 (sb, 1H, NH), 10.45 (sb, 1H, NH).

Azidation (reaction c in Extended Data Fig. 7b). To a solution of the product of the preceding step (475 mg) in dimethylformamide (24 ml), sodium azide (Sigma-Aldrich; 476 mg) was added, the reaction mixture was stirred 4 h at 100°C , and solvent was removed by rotary evaporation. ^1H -NMR (400 MHz, acetonitrile- d_3 , δ -H): 1.30 (s, 3H, CH_3), 1.50 (s, 3H, CH_3), 3.52 (d, 2H, $J = 5.3$ Hz, H-5'), 4.04 (m, 1H, H-3'), 4.69 (dd, 1H, H-4'), 4.75 (d, 1H, $J = 3.3$ Hz, H-1'), 4.87 (dd, 1H, $J = 3.3$ Hz, H-2'), 7.58 (s, 1H, H-6).

Azide reduction (reaction d in Extended Data Fig. 7b). To a solution of the crude product of the preceding step (193 mg) in tetrahydrofuran (8.8 ml) and water (1.8 ml), 1 M trimethylphosphine in tetrahydrofuran (Sigma-Aldrich; 0.74 ml) was added, the reaction mixture was stirred 2 h at room temperature, and solvent was removed by rotary evaporation. ^1H -NMR (400 MHz, D_2O , δ -H): 1.47 (s, 3H, CH_3), 1.68 (s, 3H, CH_3), 3.40 (dd, 1H, H-5'), 3.49 (dd, 1H, H-5'), 4.38 (m, 1H, H-4'), 4.90 (dd, 1H, H-1'), 4.94 (d, 1H, H-3'), 5.05 (dd, 1H, H-2'), 7.76 (s, 1H, H-6).

Fmoc protection (reaction e in Extended Data Fig. 7b). To a solution of the crude product of the preceding step (22 mg, 0.11 mmol) in dioxane (150 μ L) and water (250 μ L) sodium carbonate (26.5 mg) was added, followed by Fmoc chloride (Sigma-Aldrich; 31 mg, 1.3 eq), and the reaction mixture stirred overnight at room temperature. After addition of water (5 ml), the reaction was extracted with ethyl acetate (3 x 5 ml), the combined organic extracts were extracted with saturated sodium bicarbonate (3 x 5 ml), the combined aqueous extracts were acidified to pH 1 with 1 M HCl and extracted with ethyl acetate (3 x 5 ml), and the combined organic extracts were treated with sodium sulfate and evaporated to dryness, providing Fmoc-glycyl-L-glutamine in quantitative yield. ^1H -NMR (400 MHz, D_2O , δ -H): 1.98 (m, 1H, Asn- β), 2.18 (m, 1H, Asn- β), 2.33 (m, 2H, Asn- γ), 3.90 (m, 2H, Gly- α), 4.23 (m, 1H), 4.31 (m, 1H), 4.47 (dd, 1H, Asn- α), 7.31 (m, 2H, Ar), 7.38 (m, 2H, Ar), 7.69 (m, 2H, Ar), 7.81 (m, 2H, Ar).

Coupling, Fmoc deprotection, and formamidinylation (reactions f-h in Extended Data Fig. 7b). To a solution of the product of the preceding step (20 mg) and the product of the azide-reduction reaction (30 mg, 1.1 eq) in dry dimethylformamide (1.5 ml), N,N' -dicyclohexylcarbodiimide (Sigma-Aldrich; 18 mg, 1.2 eq) and 1-hydroxybenzotriazole (Sigma-Aldrich; 19.5 mg, 2 eq) were added, and the reaction mixture was stirred overnight at room temperature, and the solvent was evaporated under reduced pressure. To a solution of the crude coupled product (12 mg) in dimethylformamide (800 μ L), piperidine (200 μ L) was added, and the reaction mixture was stirred 10 min at 25°C , the solvent was evaporated under reduced pressure, and the residue was washed with methylene chloride (2 x 5 ml). To a solution of the crude Fmoc-deprotected product (22 mg) in methanol (300 μ L), 3,5-dimethylpyrazole-1-carboxamide (Sigma-Aldrich; 45 mg, 10 eq) was added, and the reaction mixture was stirred overnight at room temperature, followed by 6 h under reflux at 65°C to complete the reaction. The solvent was evaporated under reduced pressure, and the solid residue was washed with methylene chloride (2 x 10 ml). ^1H -NMR (400 MHz,

D₂O/CD₃OD, δ -H): 1.33 (s, 3H, CH₃), 1.54 (s, 3H, CH₃), 2.01 (m, 1H, Asn- β), 2.17 (m, 1H, Asn- β), 2.37 (m, 2H, Asn- γ), 3.37 (m, 1H, H-5'), 3.65 (m, 1H, H-5'), 4.04 (s, 2H, Gly- α), 4.03 (m, 1H), 4.11 (m, 1H), 4.42 (m, 1H), 4.63 (m, 1H), 7.53 (s, 1H, H-6).

Acetonide deprotection (reaction i in Extended Data Fig. 7b). A solution of the crude product of the preceding step (17 mg) in acetic acid:water (7:3; 2 ml) was stirred overnight at room temperature and then heated to 50°C for 10 h under argon. The solvent was evaporated under reduced pressure, and the solid residue was washed with methylene chloride (2 x 5 ml) and methanol (2 ml), yielding a white solid that, when analyzed by LC-MS [performed as described for LC-MS of PUM (Methods, Structure Elucidation of PUM); retention time = 14 min], 1D- and 2D-NMR, was indistinguishable from desoxy-PUM obtained by reduction of PUM with TiCl₃ (**1** in Extended Data Fig. 7a). ¹H-NMR (600 MHz, DMSO-d₆/D₂O, δ -H): 1.75 (m, 1H, Asn- β), 1.90 (m, 1H, Asn- β), 2.10 (m, 2H, Asn- γ), 3.29 (m, 2H, H-5'), 3.72 (m, 2H), 3.87 (s broad, 2H, Gly- α), 3.96 (m, 1H, H-2'), 4.24 (m, 1H, Asn- α), 4.40 (d, 1H, J=5.3 Hz, H-1'), 6.73 (s broad, CONH₂), 7.32 (s broad, CONH₂), 7.40 (s, 1H), 8.11 (t broad, 1H, NH), 8.34 (d broad, 1H, NH-Asn). ¹³C-NMR (DMSO-d₆, δ -H): 28.4, 31.9, 41.4, 44.0, 53.0, 72.3, 73.7, 79.9, 81.6, 110.4, 141.5, 152.2, 158.2, 164.2, 168.0, 171.3, 173.7.

Data analysis

Data for RNAP-inhibitory activities, growth-inhibitory activities, resistance, and cross-resistance are means of at least two technical replicates. Data for mouse infection models, resistance-rate assays, and checkerboard interaction assays are means and 95% confidence intervals for eight biological replicates, at least six biological replicates, and at least five technical replicates, respectively.

Data availability

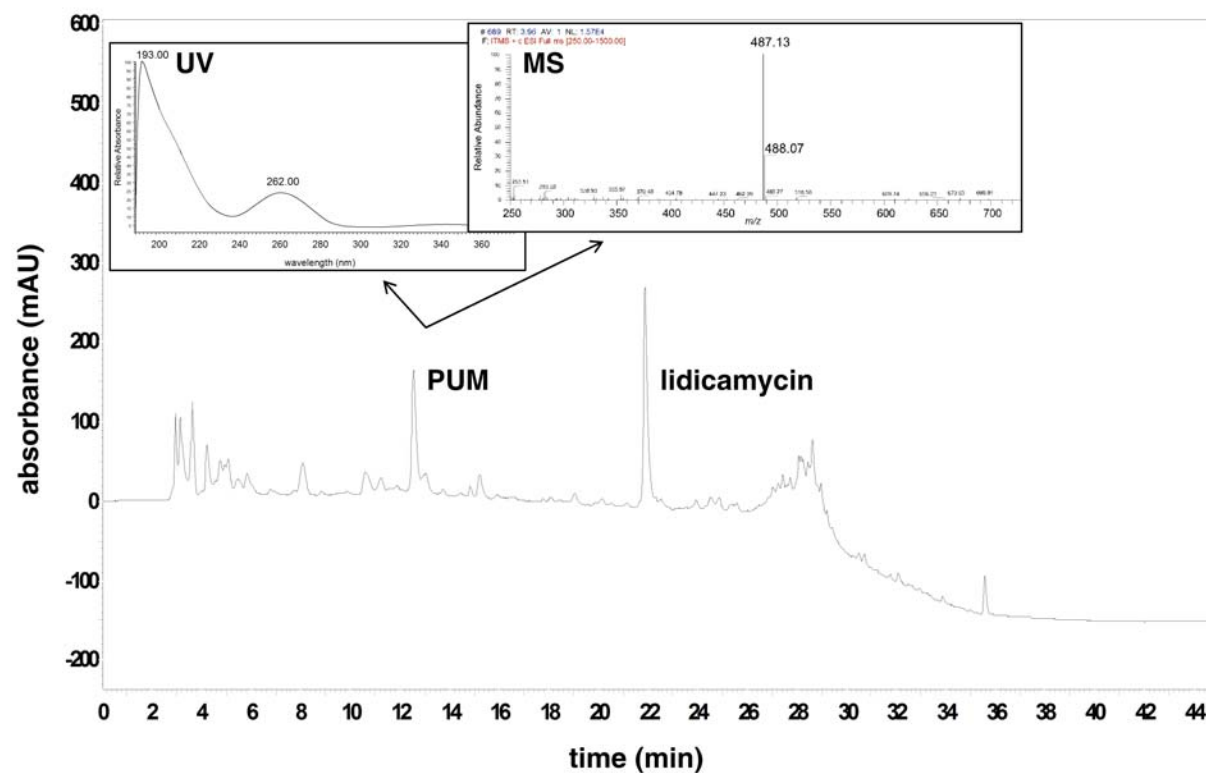
Atomic coordinates and structure factors for crystal structures of RPo-GpA-PUM and RPo-GpA-CMPcPP have been deposited in the Protein Data Bank with accession numbers 5X21 and 5X22. 16S rRNA gene sequences of PUM producer strains ID38640 and ID38673 have been deposited in GenBank with accession numbers JQ929050 and JQ929051.

REFERENCES

24. Hudson, B., Quispe, J., Lara-González, S., Kim, Y., Berman, H., Arnold, E., Ebright, R. & Lawson, C. Three-dimensional EM structure of an intact activator-dependent transcription initiation complex. *Proc. Natl. Acad. Sci. USA* **106**, 19830-19835 (2009).
25. Vrentas, C., Gaal, T., Ross, W., Ebright, R. & Gourse, R. Response of RNA polymerase to ppGpp: requirement for the ω subunit and relief of this requirement by DksA. *Genes Dev.* **19**, 2378-2387 (2005).
26. Zhang, Y., Feng, Y., Chatterjee, S., Tuske, S., Ho, M., Arnold, E. & Ebright, R. H. Structural basis of transcription initiation. *Science* **338**, 1076-1080 (2012).
27. Tang, H., Severinov, K., Goldfarb, A., Fenyo, D., Chait, B. & Ebright, R. Location, structure, and function of the target of a transcription activator protein. *Genes Dev.* **8**, 3058-3067 (1994).
28. Severinov, K., Mooney, R., Darst, S. A. & Landick, R. Tethering of the large subunits of Escherichia coli RNA polymerase. *J. Biol. Chem.* **272**, 24137-24140 (1997).
29. Niu, W., Kim, Y., Tau, G., Heyduk, T. & Ebright, R. Transcription activation at Class II CAP-dependent promoters: two interactions between CAP and RNA polymerase. *Cell* **87**, 1123-1134 (1996).
30. Qi, Y. & Hulett, F. M. PhoP~P and RNA polymerase σ^A holoenzyme are sufficient for transcription of Pho regulon promoters in *Bacillus subtilis*: PhoP~P activator sites within the coding region stimulate transcription *in vitro*. *Mol. Microbiol.* **28** (1998).
31. Donadio, S., Monciardini, P. & Sosio, M. Approaches to discovering novel antibacterial and antifungal agents. *Meths. Enzymol.* **458**, 3-28 (2009).
32. Mazza, P., Monciardini, P., Cavaletti, L., Sosio, M. & Donadio, S. Diversity of Actinoplanes and related genera isolated from an Italian soil. *Microb. Ecol.* **45**, 362-372 (2003).
33. Ploeser, J. & Loring, H. The ultraviolet absorption spectra of the pyrimidine ribonucleosides and ribonucleotides. *J. Biol. Chem.* **178**, 431-437 (1949).
34. Mattingly, P. & Miller, M. Titanium trichloride reduction of substituted N-hydroxy-2-azetidinones and other hydroxamic acids. *J. Org. Chem.* **45**, 410-411 (1980).
35. Kettenring J., Colombo, L., Ferrari, P., Tavecchia, P., Nebuloni, M., Vékey, K., Gallo, G. & Selva, E. Antibiotic GE2270A: a novel inhibitor of bacterial protein synthesis: I. structure elucidation. *J. Antibiot.* **44**, 702-715 (1991).
36. Sancar, A., Stachelejk, C., Konigsberg, W. & Rupp, Sequences of the *recA* gene and protein. *Proc. Natl. Acad. Sci. USA* **77**, 2611-2615 (1980).
37. Sambrook, J. & Russell, D. *Molecular Cloning: A Laboratory Manual* (Cold Spring Harbor Laboratory, Cold Spring Harbor, NY, 2001).
38. Schreiber, E., Matthias, P., Müller, M. & Schaffner, W. Rapid detection of octamer binding proteins with 'mini-extracts', prepared from a small number of cells. *Nucl. Acids Res.* **17**, 6419 (1989).
39. Pfleiderer, C., Smid, A., Bartsch, I. & Grummt I. An undecamer DNA sequence directs termination of human ribosomal gene transcription. *Nucl. Acids Res.* **18**, 4727-4736 (1990).
40. Dean, N. & Berk, A. (1988) Ordering promoter binding of class III transcription factors TFIIC1 and TFIIC2. *Mol. Cell. Biol.* **8**, 3017-3025.
41. Holowachuk, S., Bal'a, M. & Buddington, R. A kinetic microplate method for quantifying the antibacterial properties of biological fluids. *J. Microbiol. Meth.* **55**, 441-446 (2003).
42. Clinical and Laboratory Standards Institute (CLSI/NCCLS). *Methods for Dilution Antimicrobial Susceptibility Tests for Bacteria that Grow Aerobically; Approved Standard, Eighth Edition. CLIS Document M07-A8*. Wayne, PA. (2009).
43. Barry, A., Pfaller, M. & Fuchs, P. Haemophilus test medium versus Mueller-Hinton broth with lysed horse blood for antimicrobial susceptibility testing of four bacterial species. *Eur. J. Clin. Microbiol. Infect. Dis.* **12**, 548-553 (1993).

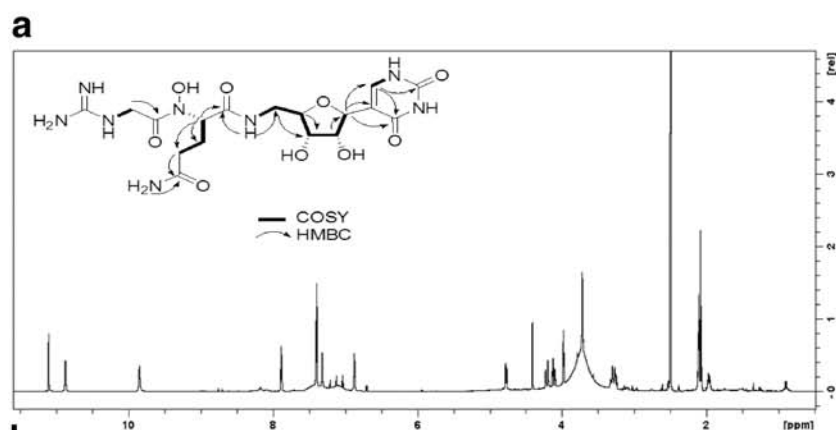
44. Mazzetti, C., Ornaghi, M., Gaspari, E., Parapini, S., Maffioli, S., Sosio, M. & Donadio, S. Halogenated spirotetronates from *Actinoallomurus*. *J. Nat. Prod.* **75** (2012).
45. Hamilton, M., Russo, R. & Thurston, R. Trimmed Spearman-Kärber method for estimating median lethal concentrations in toxicity bioassays. *Environ. Sci. Technol.* **11**, 714-719 (1977).
46. White, R., Manduru, M. & Bosso, J. Comparison of three different *in vitro* methods of detecting synergy: time-kill, checkerboard, and E test. *Antimicrob. Agents Chemother.* **40**, 1914–1918 (1996).
47. Meletiadiis, J., Pournaras, S., Roilides, E. & Walsh, T. Defining fractional inhibitory concentration index cutoffs for additive interactions based on self-drug additive combinations, Monte Carlo simulation analysis, and *in vitro-in vivo* correlation data for antifungal drug combinations against *Aspergillus fumigatus*. *Antimicrob. Agents Chemother.* **54**, 602–609. (2010).
48. Srivastava, A., Degen, D., Ebright, Y. & Ebright, R. Frequency, spectrum, and nonzero fitness costs of resistance to myxopyronin in *Staphylococcus aureus*. *Antimicrob. Agents Chemother.* **56**, 6250-6255 (2012).
49. Ma, W., Sandri, G. & Sarkar, S. Analysis of the Luria-Delbrück distribution using discrete convolution powers. *J. Appl. Probab.* **29**, 255-267 (1992).
50. Sarkar, S., Ma, W. & Sandri, G. On fluctuation analysis: a new, simple and efficient method for computing the expected number of mutants. *Genetica* **85**, 173-179 (1992).
51. Hall, B., Ma, C., Liang, P. & Singh, K. 2009. Fluctuation Analysis CalculatOR: a web tool for the determination of mutation rate using Luria-Delbrück fluctuation analysis. *Bioinformatics* **25**, 1564-1565 (2009).
52. Fralick, J. & Burns-Keliher, L. Additive effect of *tolC* and *rfa* mutations on the hydrophobic barrier of the outer membrane of *Escherichia coli* K-12. *J. Bacteriol.* **176**, 6404-6406 (1994).
53. Ebright, R. & Ebright, Y. Antibacterial agents: high-potency myxopyronin derivatives. *WO/2012037508* (2013).
54. Ciciliato, I., Corti, E., Sarubbi, E., Stefanelli, S., Gastaldo, L., Montanini, N., Kurz, M., Losi, D., Marinelli, F. & Selva, E. Antibiotics GE23077, novel inhibitors of bacterial RNA polymerase I. taxonomy, isolation and characterization. *J. Antibiot.* **57**, 210-217 (2004).
55. Wang, D., Meier, T., Chan, C., Feng, G., Lee, D. & Landick, R. Discontinuous movements of DNA and RNA in RNA polymerase accompany formation of a paused transcription complex. *Cell* **81**, 341-350 (1995).
56. Revyakin, A., Liu, C., Ebright, R. & Strick, T. Abortive initiation and productive initiation by RNA polymerase involve DNA scrunching. *Science* **314**, 1139-1143 (2006).
57. Otwinowski, Z. & Minor, W. Processing of X-ray diffraction data collected in oscillation mode. *Methods. Enzymol.* **276**, 307-326 (1997).
58. French, S. & Wilson, K. On the treatment of negative intensity observations. *Acta Cryst. D* **34**, 517-525 (1978).
59. Strong, M., Sawaya, M., Wang, S., Phillips, M., Cascio, D. & Eisenberg, D. Toward the structural genomics of complexes: crystal structure of a PE/PPE protein complex from *Mycobacterium tuberculosis*. *Proc. Natl. Acad. Sci. USA* **103** (2006).
60. Vagin, A. & Teplyakov, A. MOLREP: an automated program for molecular replacement. *J. Appl. Cryst.* **30** (1997).
61. Emsley, P., Lohkamp, B., Scott, W. & Cowtan, K. Features and development of Coot. *Acta Cryst. D* **66**, 486-501 (2010).
62. Adams, P., Afonine, P., Bunkóczi, G., Chen, V., Davis, I., Echols, N., Head, J., Hung, L., Kapral, G., Grosse-Kunstleve, R., McCoy, A., Moriarty, N., Oeffner, R., Read, R., Richardson, D., Richardson, J., Terwilliger, T. & Zwart, P. PHENIX: a comprehensive Python-based system for macromolecular structure. *Acta Cryst. D* **66**, 213-221 (2010).
63. Maffioli, S., Marzorati, E. & Marazzi, A. Mild and reversible dehydration of primary amides with PdCl₂ in aqueous acetonitrile. *Org. Lett.* **7**, 5237-5239 (2005).

64. Leitner, A. & Lindner, W. Probing of arginine residues in peptides and proteins using selective tagging and electrospray ionization mass spectrometry. *J. Mass Spectrom.* **38**, 891-899 (2003).
65. Lancini, G. & Sartori, G. Rifamycins LXI: in vivo inhibition of RNA synthesis of rifamycins. *Experientia* **24**, 1106-1106 (1968).
66. Lancini, G., Pallanza, R. & Silvestri, L. Relationships between bactericidal effect and inhibition of ribonucleic acid nucleotidyltransferase by rifampicin in *Escherichia coli* K-12. *J. Bacteriol.* **97**, 761-768 (1969).
67. Sergio, S., Pirali, G., White, R. & Parenti, F. Lipiarmycin, a new antibiotic from Actinoplanes III. Mechanism of action. *J. Antibiot.* **1975**, 543-549 (1975).
68. Irschik, H., Gerth, K., Hofle, G., Kohl, W. & Reichenbach, H. The myxopyronins, new inhibitors of bacterial RNA synthesis from *Myxococcus fulvus* (Myxobacterales). *J. Antibiot.* **36**, 1651-1658 (1983).
69. Irschik, H., Jansen, R., Hofle, G., Gerth, K. & Reichenbach, H. The corallopyronins, new inhibitors of bacterial RNA synthesis from Myxobacteria. *J. Antibiot.* **38**, 145-152 (1985).
70. Irschik, H., Augustiniak, H., Gerth, K., Hofle, G. & Reichenbach, H. The ripostatins, novel inhibitors of eubacterial RNA polymerase isolated from Myxobacteria. *J. Antibiot.* **48**, 787-792 (1995).
71. Weinzierl, R. The nucleotide addition cycle of RNA polymerase is controlled by two molecular hinges in the Bridge Helix domain. *BMC Biol.* **8**, 134 (2010).
72. Hein, P. & Landick, R. The bridge helix coordinates movements of modules in RNA polymerase. *BMC Biol.* **8** (2010).
73. Sweetser, D., Nonet, M. & Young, R. Prokaryotic and eukaryotic RNA polymerases have homologous core subunits. *Proc. Natl. Acad. Sci. USA* **84**, 1192-1196 (1987).
74. Lane, W. & Darst, S. Molecular evolution of multisubunit RNA polymerases: sequence analysis. *J. Mol. Biol.* **395**, 671-685 (2010).
75. Jokerst, R., Weeks, J., Zehring, W., & Greenleaf, A. Analysis of the gene encoding the largest subunit of RNA polymerase II in *Drosophila*. *Mol. Gen. Genet.* **215**, 266-275 (1989).



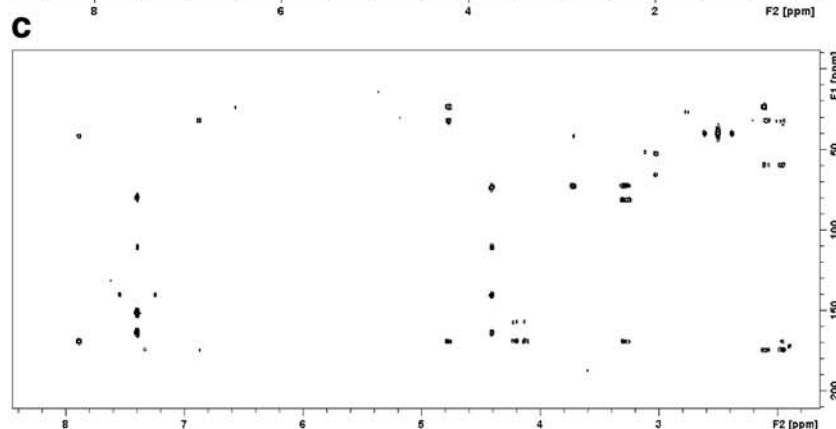
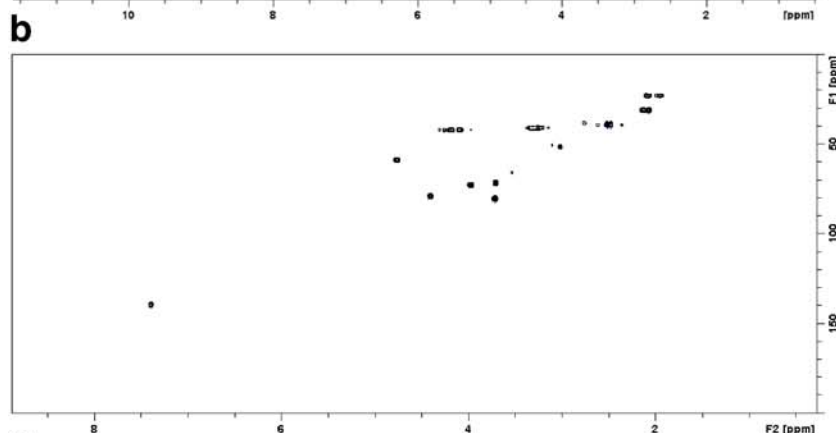
Extended Data Figure 1. Isolation of PUM.

Chromatographic profile of *Streptomyces* sp. ID38640 culture extract, showing peaks for PUM and lidicamycin, and UV-absorbance and mass spectra for PUM.



Extended Data Figure 2. Structure elucidation of PUM.

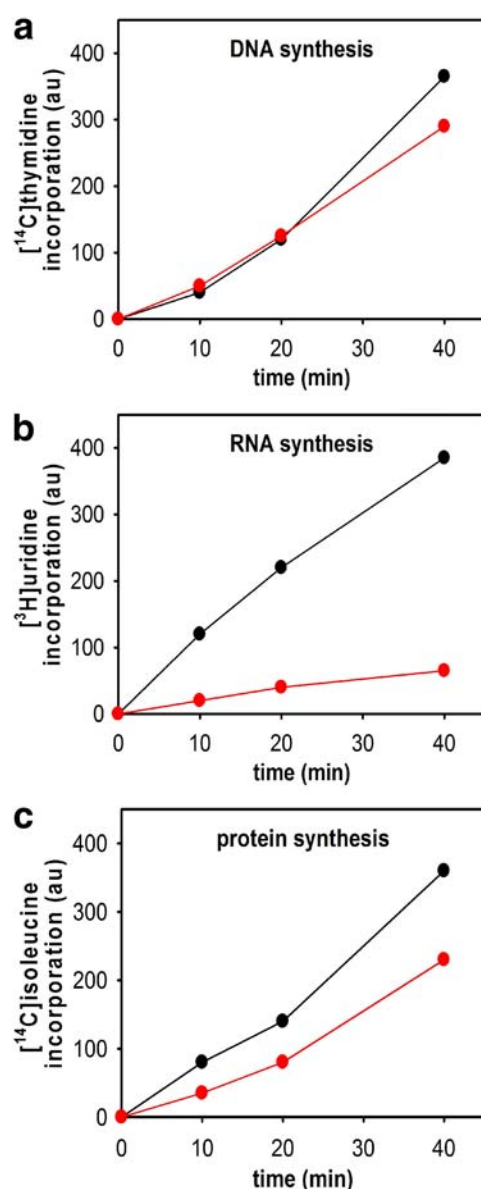
a, Structure and ^1H -NMR spectrum of PUM in DMSO-d_6 at 25°C at 400 MHz. **b**, 2D-HSQC spectrum of PUM in DMSO-d_6 at 25°C at 400 MHz. **c**, 2D-HMBC spectrum of PUM in DMSO-d_6 at 25°C at 400 MHz. **d**, Summary of ^1H -, ^{13}C -, and ^{15}N -NMR data for PUM in DMSO-d_6 .



d

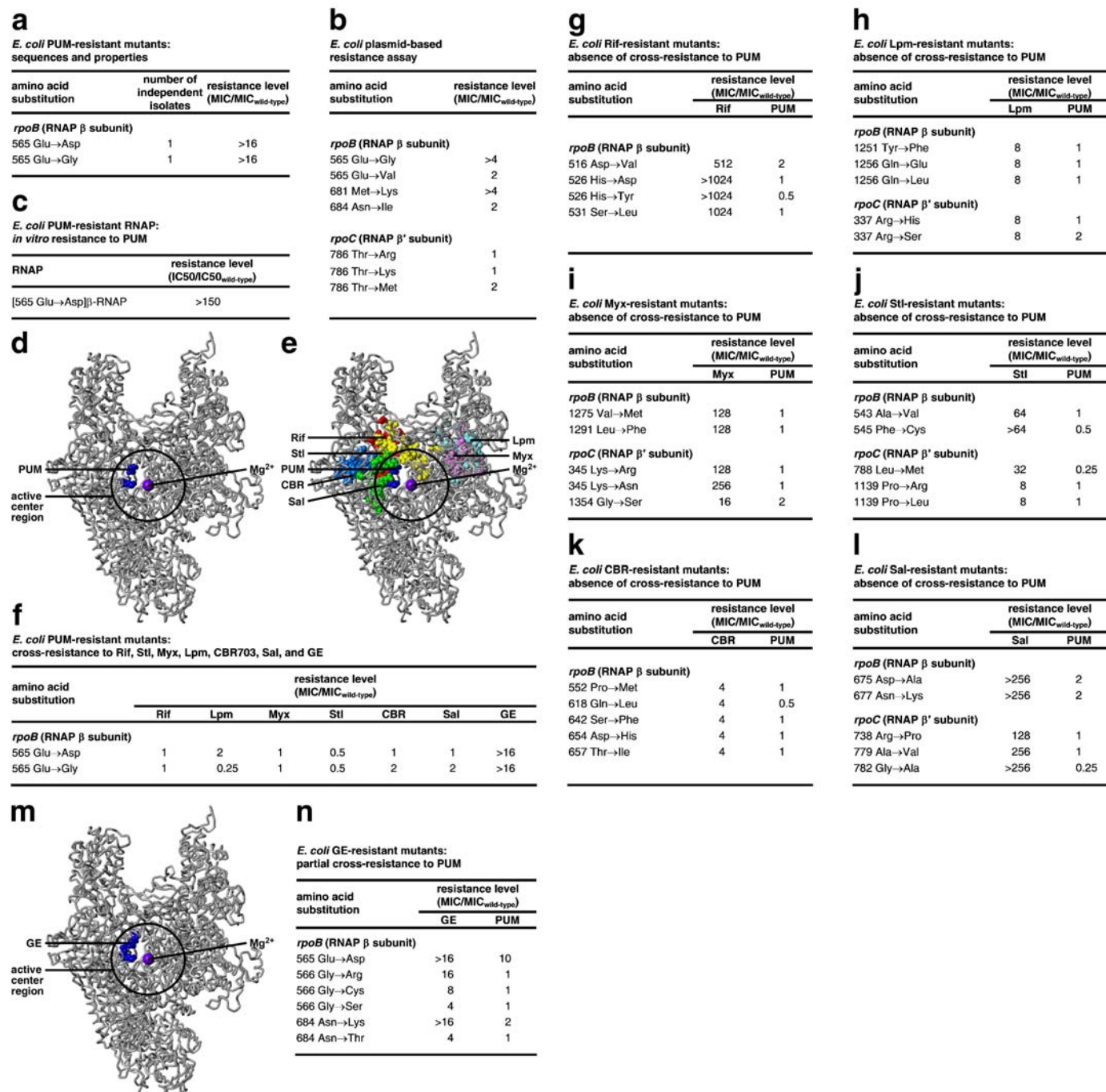
^1H -, ^{13}C -, and ^{15}N -NMR data of PUM in DMSO-d_6 at 25°C

		^1H (δ , ppm), multiplicity (J [Hz])	^{13}C (δ , ppm)	^{15}N (δ , ppm)
ribose	1'	4.34, d (4.70)	79.8	
	2'	3.91, dd (4.70, 5.32)	73.8	
	3'	3.65, m	76.3	
	4'	3.65, m	81.4	
	5'	3.24, m; 3.14, m	42	
	6'	7.82, t (5.62)		108.5
pseudouridine	1		110.7	
	2		164	
	3	11.04, d (1.92)		158.5
	4		152	
	5	10.8, dd (1.64)		131
	6	7.33, d (1.62)	140.4	
Gln	C=O		169.5	
	α	4.72, m	59	
	β	2.03, m; 1.90, m	23.6	
	γ	2.04, m; 1.91, m	31.7	
	δ		174	
Gly	N ϵ	7.26, bs; 6.81, bs		108.9
	NH	7.43, dd (4.95, 5.06)		75.1
	C=O		157	
	α	4.22, m; 4.12, m	43	



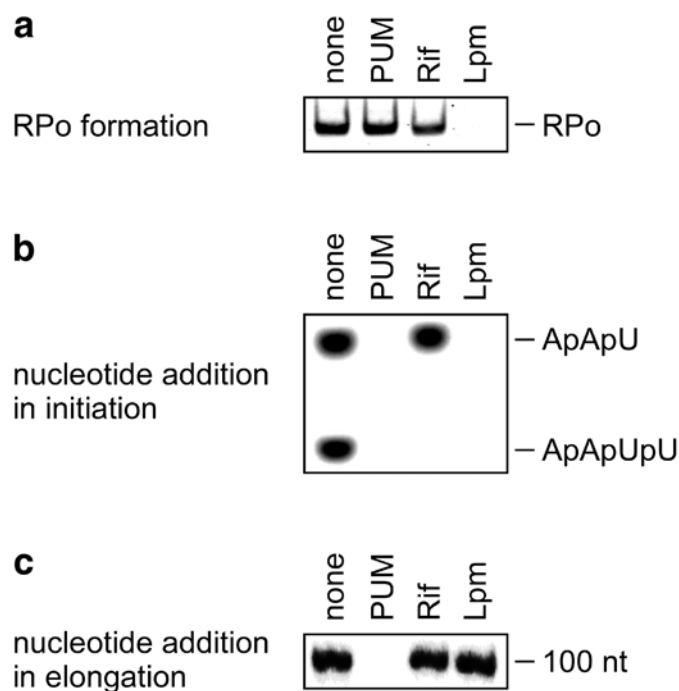
Extended Data Figure 3. Effects of PUM on macromolecular synthesis in bacterial cells in culture: inhibition of RNAP-dependent RNA synthesis.

Effects of PUM on DNA synthesis (**a**; [¹⁴C]-thymidine incorporation), RNA synthesis (**b**; [³H]-uridine incorporation), and protein synthesis (**c**; [¹⁴C]-isoleucine incorporation) in *Staphylococcus simulans* in culture. Results match characteristic pattern for inhibition of RNAP-dependent RNA-synthesis^{18,65-70}: i.e., rapid and strong inhibition of RNA synthesis, slower and weaker inhibition of protein synthesis, and little or no inhibition of DNA synthesis.



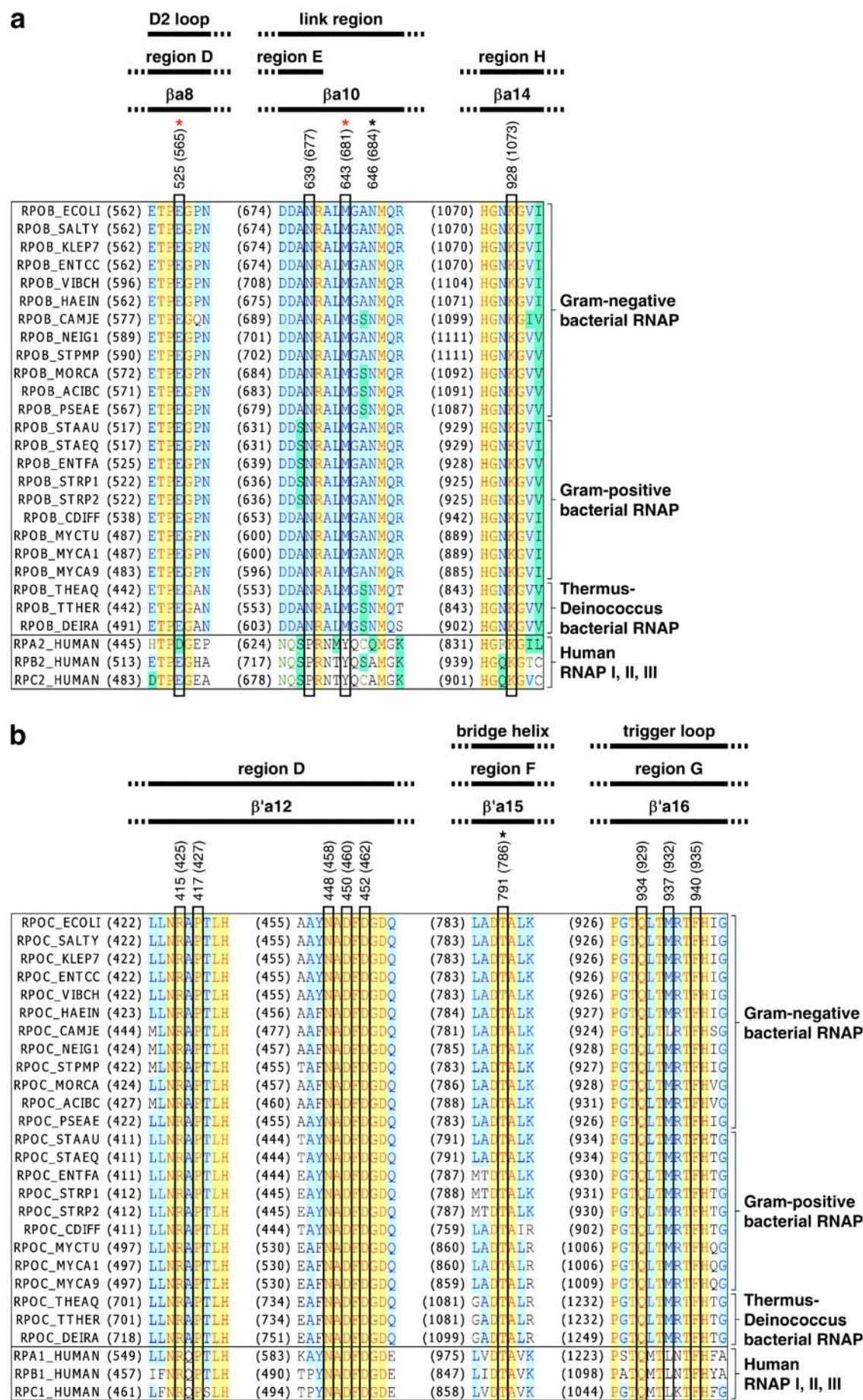
Extended Data Figure 4. Target of PUM: RNAP i+1 NTP binding site: results for Gram-negative bacterium *E. coli*.

a, *E. coli* spontaneous PUM-resistant mutants. **b**, Effects of *S. pyogenes* PUM-resistant mutants (sequences from Fig. 2b) when analyzed in *E. coli* plasmid-based resistance assay. Two substitutions confer moderate or higher (≥ 4 x) resistance in *E. coli* plasmid-based resistance assay: $\beta 565$ Glu→Gly and $\beta 681$ Met→Lys. **c**, PUM-resistant phenotype of purified *E. coli* RNAP containing $\beta 565$ Glu→Asp. **d**, Location of *E. coli* PUM target (sequences from **a-b**) in three-dimensional structure of bacterial RNAP (colors as in Fig. 2c). **e**, Absence of overlap between PUM target (blue) and Rif (red), Lpm (cyan), Myx (pink), Stl (yellow), CBR (light blue), and Sal (green) targets. **f**, Absence of cross-resistance of *E. coli* PUM-resistant mutants (sequences from **a-b**) to Rif, Lpm, Myx, Stl, CBR, and Sal. **g-l**, Absence of cross-resistance of *E. coli* Rif-, Lpm-, Myx-, Stl-, CBR-, and Sal-resistant mutants to PUM. **m**, Location of GE target (blue) in structure of bacterial RNAP. PUM target (**d**) shows partial overlap with GE target (**m**). **n**, Partial cross-resistance of *E. coli* GE-resistant mutants to PUM.



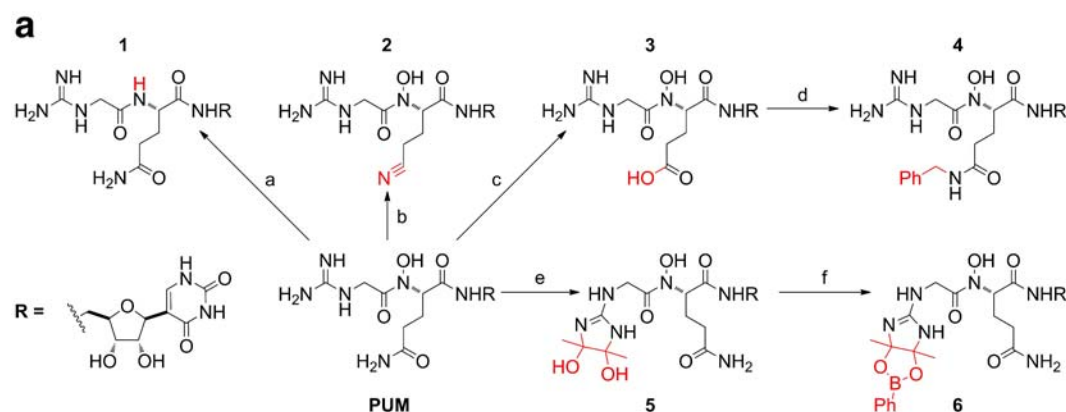
Extended Data Figure 5. Mechanism of PUM: inhibition of nucleotide addition

a, Absence of inhibition by PUM of formation of catalytically-competent RNAP-promoter open complex (RPo). **b**, Inhibition by PUM of nucleotide addition in transcription initiation. **c**, Inhibition by PUM of nucleotide addition in transcription elongation.

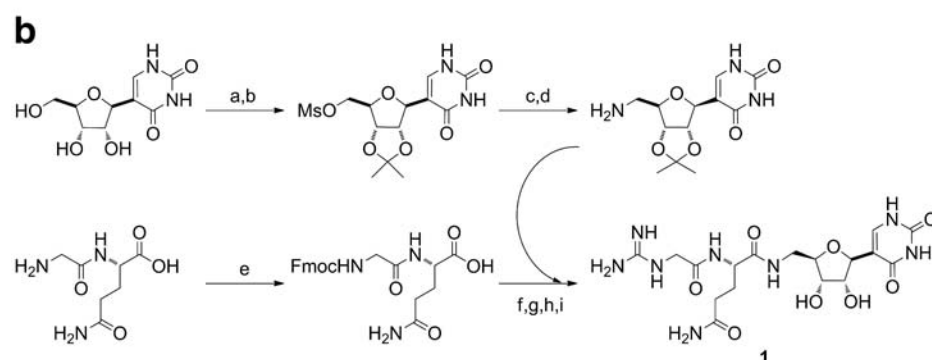


Extended Data Figure 6. Interactions between RNAP and PUM: sequence alignments.

Locations of residues that contact PUM in the sequences of RNAP β subunit (a) and RNAP β' subunit (b). Sequence alignments for β and β' subunits of bacterial RNAP (top 24 sequences in each panel) and corresponding subunits of human RNAP I, RNAP II, and RNAP III (bottom three sequences in each panel), showing locations of RNAP residues that contact PUM (black rectangles; numbered as in *S. pyogenes* and, in parentheses, as in *E. coli*; identities from Fig. 4a), locations of residues at which substitutions conferring PUM-resistance are obtained in both *S. pyogenes* and *E. coli* (red asterisks; identities from Fig. 2b and Extended Data Fig. 4a-b), locations of residues at which substitutions conferring PUM-resistance are obtained in *S. pyogenes* but not *E. coli* (black asterisks; identities from Fig. 2b and Extended Data Fig. 4a-b), locations of RNAP structural elements⁷¹⁻⁷² (top row of black bars), and RNAP conserved regions⁷³⁻⁷⁵ (next two rows of black bars). Species are as follows: *E. coli* (ECOLI), *Salmonella typhimurium* (SALTY), *Klebsiella pneumoniae* (KLEP7), *Enterococcus cloacae* (ENTCC), *Vibrio cholerae* (VIBCH), *Haemophilus influenzae* (HAEIN), *Campylobacter jejuni* (CAMJE), *Neisseria gonorrhoeae* (NEIG1), *Stenotrophomonas maltophilia* (STPMP), *Moraxella catarrhalis* (MORCA), *Acinetobacter baumannii* (ACIBC), *Pseudomonas aeruginosa* (PSEAE), *Staphylococcus aureus* (STAAU), *Staphylococcus epidermidis* (STAEQ), *Enterococcus faecalis* (ENTFA), *Streptococcus pyogenes* (STRP1), *Streptococcus pneumoniae* (STRP2), *Clostridium difficile* (CDIFF), *Mycobacterium tuberculosis* (MYCTU), *Mycobacterium avium* (MYCA1), *Mycobacterium abscessus* (MYCA9), *Thermus aquaticus* (THEAQ), *Thermus thermophilus* (THETH), *Deinococcus radiodurans* (DEIRA), and *Homo sapiens* (HUMAN).



(a) TiCl_3 , 1M NaOAc (pH 7), RT 2h, 100%; (b) PdCl_2 , 1:1 ACN: H_2O , RT 2h, 90%; (c) 0.1% TFA, RT 3 days, 100%;
 (d) BnNH_2 , DMF + PyBOP, RT 30min, 100%; (e) 2,3-butanedione, 10mM NH_4OAc (pH 8), RT 30min, 100%;
 (f) PhB(OH)_2 , 10 mM NH_4OAc (pH 8), RT 2h, 100%



(a) $\text{Me}_2\text{C(OMe)}_2$, DMF, HCl, RT 5h, 100%; (b) MsCl , Pyr, 0°C + RT 16h, 95%; (c) NaN_3 , DMF, 100°C 4h, 86%;
 (d) Me_3P , THF + H_2O , RT 2h, 95%; (e) Na_2CO_3 + FmocCl , dioxane + H_2O , RT o/n, 100%;
 (f) DCC-HOBT, dry DMF, RT o/n, 95%; (g) piperidine, DMF, 25°C 10min, 100%;
 (h) 3,5-dimethylpyrazole-1-carboxyamidine, MeOH, RT o/n + 65°C 6h, 100%;
 (i) 7:3 $\text{AcOH-H}_2\text{O}$, RT o/n + 50°C 10h under Ar, 100%

c
RNAP-inhibitory activity (*E. coli* RNAP)

PUM derivative	IC ₅₀ (μM)
PUM	0.3
1	4
2	>50
3	4
4	1
5	>50
6	>50

d
antibacterial activity (*S. pyogenes*)

PUM derivative	MIC (μg/ml)
PUM	2
1	16
2	>64
3	16
4	16
5	>64
6	>64

Extended Data Figure 7. Semi-synthesis, synthesis, and analysis of PUM derivatives.

a, Semi-synthesis of PUM derivatives lacking PUM N-hydroxy group (**1**), having alterations of PUM glutaminyl sidechain (**2-4**), or having alterations of PUM guanidinyl sidechain (**5-6**). **b**, Synthesis of PUM derivative lacking PUM N-hydroxy group (**1**). **c-d**, RNAP inhibitory activities and antibacterial activities of PUM derivatives.

Extended Data Table 1. Selectivity of RNAP-inhibitory activity

enzyme	IC50 (μM) (± SEM)	selectivity ratio
promoter-dependent transcription		
<i>E. coli</i> RNAP		
6.25 μM UTP	0.1	[1]
50 μM UTP	2	[1]
250 μM UTP	8	[1]
human RNAP I		
6.25 μM UTP	>50	>500
50 μM UTP	ND	ND
250 μM UTP	ND	ND
human RNAP II		
6.25 μM UTP	1	10
50 μM UTP	7	4
250 μM UTP	>20	>3
human RNAP III		
6.25 μM UTP	9	90
50 μM UTP	ND	ND
250 μM UTP	ND	ND
promoter-independent transcription		
<i>E. coli</i> RNAP		
1.56 μM UTP	0.9 (± 0.1)	[1]
25 μM UTP	4 (± 0.7)	[1]
400 μM UTP	10 (± 2)	[1]
HeLa nuclear extract (human RNAP I / II / III)		
1.56 μM UTP	4 (± 0.1)	4
25 μM UTP	15 (± 6)	4
400 μM UTP	51 (± 30)	5

Extended Data Table 2. Antibacterial activity *in vivo* (mouse *S. pyogenes* peritonitis model; 7 day survival)

intravenous (iv) administration, 10 min and 6 h post-infection		intravenous (iv) administration, 10 min post-infection		subcutaneous (sc) administration, 10 min post-infection	
PUM total dose (mg/kg)	survivors / total	PUM total dose (mg/kg)	survivors / total	PUM total dose (mg/kg)	survivors / total
50	7 / 8	40	5 / 8	40	6 / 8
20	6 / 8	16	4 / 8	16	2 / 8
8	5 / 8	6.4	0 / 8	6.4	1 / 8
3.2	0 / 8	2.56	2 / 8	2.56	1 / 8
0	0 / 8	1.024	0 / 8	1.024	0 / 8
		0	0 / 8	0	0 / 8

Extended Data Table 3. Data collection and refinement statistics.

	RPo-GpA-PUM (5X21)	RPo-GpA-CMPcPP (5X22)
Data collection		
Space group	C2	P2 ₁
Cell dimensions		
<i>a</i> , <i>b</i> , <i>c</i> (Å)	186.8, 103.1, 296.2	186.4, 104.3, 297.3
α , β , γ (°)	90.0, 98.7, 90.0	90.0, 98.4, 90.0
Resolution (Å)	40.00-3.30 (3.36-3.30)*	50.00-3.35 (3.41-3.35)*
<i>R</i> _{sym} or <i>R</i> _{merge}	0.138 (0.633)	0.197 (>1.0)
<i>I</i> /σ(<i>I</i>)	8.4 (1.7)	7.7 (1.8)
Completeness (%)	0.920 (0.874)	0.956 (0.891)
Redundancy	3.4 (3.4)	5.3 (5.3)
Refinement		
Resolution (Å)	50.00-3.32	50.00-3.33
No. reflections	70085	147976
<i>R</i> _{work} / <i>R</i> _{free}	0.232/0.280	0.208/0.250
Number of atoms		
Protein/DNA/RNA	28662	56787
Ligand/ion	42	76
Water	35	0
<i>B</i> factors		
Protein	61.6	41.8
Ligand/ion	31.8	21.0
Water	34.3	-
R.m.s deviations		
Bond lengths (Å)	0.002	0.007
Bond angles (°)	0.542	0.834

*Values in parentheses are for highest-resolution shell.